

2016

Modeling Transport Phenomena in Solid-State Polymer Processing

Evan Vincent Miu

Bucknell University, evm004@bucknell.edu

Follow this and additional works at: https://digitalcommons.bucknell.edu/honors_theses

Recommended Citation

Miu, Evan Vincent, "Modeling Transport Phenomena in Solid-State Polymer Processing" (2016). *Honors Theses*. 352.
https://digitalcommons.bucknell.edu/honors_theses/352

This Honors Thesis is brought to you for free and open access by the Student Theses at Bucknell Digital Commons. It has been accepted for inclusion in Honors Theses by an authorized administrator of Bucknell Digital Commons. For more information, please contact dcadmin@bucknell.edu.

Modeling Transport Phenomena in Solid-State Polymer Processing

by

Evan V. Miu

A Thesis Submitted to the Honors Council
For Honors in Chemical Engineering

May 2nd, 2016

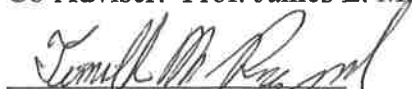
Approved by:



Co-Adviser: Prof. Katsuyuki Wakabayashi



Co-Adviser: Prof. James E. Maneval



Department Chairperson: Prof. Timothy M. Raymond

Acknowledgements

I would first like to thank my advisers, Dr. Maneval and Dr. Wakabayashi, for their unwavering support throughout the past year. Dr. Maneval has consistently challenged me to push my limits, and I have developed nothing but the utmost respect for him. I am grateful for his unparalleled insight, and cannot begin to express my appreciation of his ability to make the most difficult things seem so simple. Dr. Wakabayashi has also been an invaluable adviser, even from over 3,000 miles away. His constant questioning and his exacting attention to detail have helped me become a better, clearer thinker. Kat has been one of my best friends at Bucknell, and I am thankful for his unwavering loyalty and support. Without the patience and guidance of both of my advisers, I would not be the student or person that I am today.

Furthermore, I would like to thank my friends for always reminding me there is more to college than school work. As much as I enjoy research and learning, I cannot say I was ever unhappy when I was convinced to not do work. A special thank you to Jenn Rich, Christian Cavarretta, and Margot Farnham.

Finally, and most importantly, I would like to thank my parents. My parents are the most knowledgeable and resourceful people I know, and without their support I would not be where I am today. I would like to thank them for teaching me to “think.”

Table of Contents

Acknowledgements	iv
List of Tables	vi
List of Figures	vii
List of Variables	x
Abstract	xiii
1. Introduction	1
2. Background	7
2.1 Methods of Extrusion.....	7
2.2 Instrumentation	10
2.3 Heat Transfer within SSSP	14
3. Problem Definition and Modeling Approach	18
3.1 Overarching Goals of the Thesis.....	18
3.2 Modeling Technique	19
4. Development of Velocity Profiles	23
4.1 Conveying Elements	23
4.2 Kneading Elements	38
5. Development of Temperature Profiles	48
5.1 Conveying Elements	48
5.2 Kneading Elements	66
6. Comparisons and Future Work	73
6.1 Comparisons	73
6.2 Future Work	75
7. References	81
8. Appendix A: Discussion of Pressure Effects on Velocity and Temperature Profiles	85
A.1 Development of Velocity Profiles for Varying Pressure Effects	85
A.2 Development of Temperature Profiles for Varying Pressure Effects	86
9. Appendix B: Discussion of Heat Generation, Ω	90

List of Tables

Table 5.1.1: Decomposition to ODE and PDE problems	56
Table 5.1.2: First eight eigenvalues and corresponding constants.....	62
Table 5.1.3: Average values of the first eight eigenfunctions for conveying element flow	64
Table 5.2.1: Decomposition to ODE and PDE problems	68
Table B.1.1: First eight eigenvalues and corresponding constants	87

List of Figures

Figure 1.1: SSSP / SSME instrumentation at Bucknell University	2
Figure 1.2: Energy flows characteristic of twin screw extrusion methods	4
Figure 2.1.1: Typical single screw extrusion set up (top-view).....	7
Figure 2.1.2: Typical twin screw extrusion setup (top-view)	8
Figure 2.1.3: Typical solid-state shear pulverization setup (top-view)	9
Figure 2.2.1: The KMB ZE-25 UTX extruder at Bucknell University.....	10
Figure 2.2.2: Various classifications of twin screw machines.....	11
Figure 2.2.3: Conveying elements used in Bucknell’s SSSP machine.....	12
Figure 2.2.4: Kneading elements used in Bucknell’s SSSP machine	12
Figure 2.2.5: Cross section of the ZE-25 extruder barrels	13
Figure 2.2.6: Location of the cooling lines	13
Figure 2.3.1: Overall, general energy balance for SSSP system	15
Figure 3.2.1: Representation of an arbitrary volume of material moving through space and time.....	19
Figure 4.1.1: Conveying elements used in Bucknell’s SSSP machine	24
Figure 4.1.2: Screw element with cylindrical and Cartesian coordinates.....	25
Figure 4.1.3: Cross-sectional view of intermeshed co-rotating twin-screws.....	26
Figure 4.1.4: Representation of parallel plate flow in an unwound SSSP conveying element.....	27
Figure 4.1.5: Flattened surface of a conveying element	32
Figure 4.1.6: Cross section of one of the twin-screws, showing Zones 1 and 2.....	34

Figure 4.1.7: Unwound screw representation of the two flow regions in a conveying element.....	34
Figure 4.1.8: Representation of the effective velocity profile	35
Figure 4.1.9: Shape of the effective conveying velocity profile.....	38
Figure 4.2.1: Kneading elements used in Bucknell’s SSSP machine	39
Figure 4.2.2: Illustration of the cylindrical coordinate system assigned to kneading elements	39
Figure 4.2.3: Axial view of the “smoothed” kneading element-barrel system.....	40
Figure 4.2.4: Circumferential velocity profile for kneading discs.....	43
Figure 4.2.5: General shape of the axial pressure driven velocity profile in kneading elements	45
Figure 5.1.1: Péclet versus Graetz flow types.....	54
Figure 5.1.2: First eight eigenfunctions that contribute to the series solution for $X(\xi')$ for $\beta = 0$	62
Figure 5.1.3: $[\sum_{n=1}^8 A_n F_n(\lambda_n; \xi')]$ Sum of the first eight eigenfunctions that contribute to the solution for $X(\xi')$ for $\beta = 0$	63
Figure 5.1.4: Comparison of the effectiveness of various series solutions for $\beta = 0$	65
Figure 6.2.1: Screw design used in this study.....	77
Figure 6.2.2a: Experimental temperature measurements for varying flow rates.....	77
Figure 6.2.2b: Experimental temperature measurements for varying screw speeds.....	78
Figure 6.2.3a: Temperature predictions for various feed rates; arrows point to kneading zones	79
Figure 6.2.3b: Temperature predictions for varying screw speeds; arrows point to kneading zones.....	79
Figure A.1.1: Dimensionless velocity profiles for various values of β	85
Figure A.2.1: First eight eigenfunctions that contribute to the series solution for $X(\xi')$ for $\beta = 1$	87

Figure A.2.2: $[\sum_{n=1}^8 A_n F_n(\lambda_n; \xi')]$ Sum of the first eight eigenfunctions that contribute to the solution for $X(\xi')$ for $\beta = 1$ 88

Figure A.2.3: Comparison of the effectiveness of various series solutions for $\beta = 1$ 88

List of Variables

A_n	=	Constant of integration
α	=	Angle of rotation
β	=	Dimensionless pressure vs. drag flow
c_i	=	Constant of integration
\hat{C}_p	=	Heat capacity
D	=	Diameter of screw
Δ	=	Delta
F_n	=	Eigenfunction
g	=	Gravitational force
∇	=	Gradient
H	=	Channel height
ξ	=	Dimensionless channel height
η	=	Viscosity
J_p	=	Bessel function of order p
k	=	Thermal conductivity
κ	=	Ratio of inner to outer radius
L	=	Channel length
ζ	=	Dimensionless channel length
λ_n	=	Eigenvalue
\dot{m}	=	Mass flow rate

N	=	Screw rotation rate
P	=	Pressure
Γ	=	Dimensionless pressure
ρ	=	Density
ψ	=	Dimensionless arbitrary heat generation
Φ_v	=	Viscous dissipation function
φ	=	Fraction of rotation
ϕ	=	Flight angle
R	=	Screw radius
γ	=	Dimensionless radius
S	=	Arbitrary heat generation
S_c	=	Scale heat generation
t	=	Time
T	=	Temperature
T_b	=	Barrel temperature
T_s	=	Screw temperature
T_o	=	Initial temperature
τ	=	Stress
θ	=	Dimensionless temperature
θ_o	=	Dimensionless initial temperature
\dot{v}	=	Volumetric flow rate
v_i	=	Velocity

V_i	=	Directionally specific scale velocity
v_s	=	Scale velocity
$\langle v \rangle$	=	Average velocity
μ	=	Viscosity
U	=	Dimensionless velocity
W	=	Channel width
ω	=	Dimensionless channel width
Ω	=	Heat generation and heat conduction (pseudo-Brinkman number)
Ω_o	=	Angular velocity

Abstract

Polymer processing techniques make and shape many of the products we use in our daily lives. Solid-state shear pulverization (SSSP) is a novel extrusion technique that has been shown to produce materials that have been historically difficult to manufacture, and has opened a new door to unique polymer products. The process employs cold temperatures and pulverizes solid plastics into fine powders, achieving morphological changes and physical property improvements via mechanochemical reactions. These reactions, along with concurrent solid-state interactions, generate a significant amount of heat. The interplay of this heat and cooling by the instrument formulates a unique heat transfer setting.

Understanding the intricate heat transfer phenomena in SSSP should rely on quantitative modeling, rather than trial-and-error methodologies. Previous modeling studies of similar extrusion systems have applied continuum mechanics as the basis, simultaneously considering the transfer of momentum, heat, and mass. Solving the balance equations leads to the development of functions that describe velocity and temperature within a given system.

This thesis applies the modeling techniques of continuum mechanics to SSSP with the goal of quantifying heat transfer characteristics within the extruder system. First, profiles of velocity for the varying screw element types are developed. The resulting velocity profiles suggest flow within the extruder is a combination of drag and pressure flows. Then, temperature profiles are constructed for each element type. The profiles describe the behavior of temperature within a single screw element, and show that the

system is of Graetz type flow. This study provides the necessary tools for compiling a temperature profile that describes the entire extruder, lending insight into the process parameters and material properties that are significant to the generation and removal of heat in the system.

1. Introduction

Polymers are materials that have formed the functional backbone of modern society; they house our most delicate electronics, support our tallest mega-structures, and show promise in many biomedical applications. Polymers are effective because they can be processed in different physical and chemical ways. Physical processing, such as injection- and compression-molding, focuses on altering the shape and dimensions of a polymer. These physical modifications affect the material's properties in a macroscopic and extrinsic fashion. For example, a single material can be made pliable and weak if it is thin, or strong and stiff if it is thick. In contrast, chemical processing, such as oxidation or vulcanization, alters the micro- and nano-scale structure of a polymer. These intrinsic modifications follow the fundamental structure-property relations of macromolecular science to affect the material's behavior throughout all scales. Using a combination of chemical and physical processes allows for meticulous product design tailored to specific applications.

Solid-state processing is a relatively new category of polymer processing developed in the late 1990's, which is gaining significant scientific and industrial traction [1]. There have been over 50 journal papers and more than 20 patents covering this single technology. Originating from Northwestern University, the extruder-based solid-state technology encompasses solid-state shear pulverization (SSSP) and now solid-state/ melt extrusion (SSME), which was recently developed at Bucknell University. Institutionally, solid-state polymer processing is only available at these two universities. Figure 1.1 is an image of the extruder-based instrument for conducting SSSP and SSME.

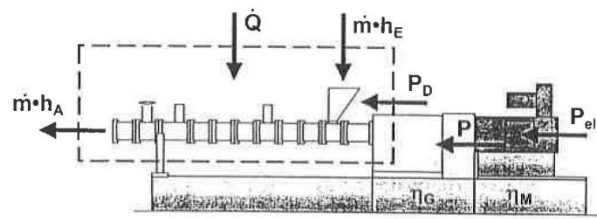


Figure 1.1: SSSP / SSME instrumentation at Bucknell University

Solid-state processing is extremely unique because of its drastically different approach of treating and mixing materials. In contrast to the traditional means of melt extrusion and compounding, which heats the material being processed (to allow for fluid phase mixing and kneading), solid-state processing cools the material and prevents melting, and therefore instigates intense mechanical shearing and compression between individual particles. These characteristic solid-solid interactions allow for the development of mechanochemical phenomena, through which the material's physical morphology and chemical structure are simultaneously altered. Mechanochemical effects observed in polymers include chain scission, free-radical formation, short-chain branching, and inter-chain cross linking [2-4]. These mechanochemical effects in turn lead to favorable macroscopic changes in the materials, such as immiscible phase compatibilization, increased composite filler exfoliation, and increased blend phase dispersion [5, 6]. Based on these mechanochemical concepts, both SSSP and SSME

techniques have been successful in fabricating a wide range of polymer-based materials more effectively and efficiently than traditional processing methods. Homopolymer systems processed in the solid-state, such as polypropylene and polylactic acid, have been shown to exhibit improved material properties and crystallization kinetics [7, 8]. Polymer nanocomposites (PNCs) have also been effectively produced via solid-state extrusion; linear low density polyethylene-montmorillonite clay, polypropylene-graphite, and polypropylene-carbon nanotube PNCs all showed increases in material properties after solid-state processing [4, 9, 10]. SSSP and SSME have also shown promise in plastics recycling applications, namely in the recycling of high density polyethylene, polypropylene, and several other commingled postconsumer plastic mixtures [11, 12]. Polypropylene-eggshell biocomposites have been successfully developed using SSSP, as well as ultra-high molecular weight polyethylene / high density polyethylene composites [13, 14].

Solid-state processing has one very important working principle: in order to induce sufficient levels of shear and compression to properly alter the material, the process must be at a low temperature, and the materials must be in the solid-state phase. Relying on this principle is a difficult task, because the process involves an intricate balance of energy and heat inputs and outputs, as seen below in Figure 1.2.



Energy balance: $P_D + \dot{Q} = \dot{m} \cdot \Delta h$

Dissipated drive power: $P_D = \eta_M \cdot \eta_G \cdot P_{el}$ $\eta_M, \eta_G \approx 0,94 \dots 0,96$

Heat transfer: $\dot{Q} = k \cdot A \cdot (T_{TM} - T_M)$

Drive power: $P = \eta_M \cdot P_{el} = P_D / \eta_G$

Figure 1.2: Energy flows characteristic of twin screw extrusion methods [11]

To date, there has been little to no theoretical modeling performed on the process. There has been limited effort in quantifying the process parameters which govern heat transfer in solid-state extruders, or to model the effects of temperature and velocity distributions in the equipment. Energy balances have been considered for the SSSP process on the macroscopic scale in terms of motor and chiller energies, as seen in Figure 1.2 [11], but there have been no efforts to understand heat and momentum transfer characteristics of SSSP or SSME from a more fundamental, small-scale perspective. Because no adequate models exist to completely explain the transport phenomena within the flowing material, SSSP and SSME research has relied on past experience and trial-and-error work. In addition, the exotic nature of the SSSP and SSME processes often attracts skepticisms and criticisms of the validity of the processes. Academics and industrial experts often question the cooling ability of the solid-state extruder. Cooling capacity, efficiency, and feasibility are almost universally debated when solid-state

technologies are introduced. Considering the broad potential of SSSP and SSME to develop a wide range of polymeric materials, a fundamental understanding of the process is needed.

The proposed research study aims to theoretically model the heat transfer characteristics in solid-state polymer processing techniques. Fundamental chemical engineering principles of conservation and transport will be used to analyze the extruder system on different size scales. The developed model will effectively describe temperature profiles and heat transfer within the solid-state extruder through theoretical analyses. By understanding the interplay of process parameters, material properties, flow profile, and temperature profile, melt transition events could theoretically be predicted in SSSP and SSME. The work will not only provide quantitative answers to various inquiries, skepticisms, and criticisms from the members of the research community, but it will allow a better fundamental understanding of the process, and provide avenues of process optimization. The results are expected to strengthen the case for the commercial use of solid-state processing methods, allowing for the possible growth of SSSP and SSME as industrially viable processes.

This Honor's thesis is structured to provide an in-depth and transparent study of transport phenomena within solid-state extrusion. Chapter 2 describes the general setup and functionality of Bucknell University's twin screw extruder. Chapter 3 discusses relevant background theory and develops thesis questions that explicitly frame the main research work. The main investigation of the thesis is done in two steps. Chapter 4 constitutes the first major step, and develops velocity profiles within the extruder.

Chapter 5 then moves on to the second step, which concerns the development of temperature profiles within the extruder. Chapter 6 summarizes the key findings of the study and provides recommendations for the best way to apply the modeling results to future research in this field.

2. Background

2.1. Methods of Extrusion

Solid-state shear pulverization is a variation of a type of polymer processing known as screw extrusion. Screw extrusion has been used since the 19th century [15-17]. Single screw extrusion (SSE), the most fundamental screw extrusion method first patented in the 1870's, consists of a singular rotating screw housed inside a stationary heated barrel; material is fed to the upstream side of the screw, and is pumped down the length of the machine. Figure 2.1.1 is a schematic of a single screw extruder.



Figure 2.1.1: Typical single screw extrusion set up (top-view)

The screws in SSE instruments are helical conveying screws. As the screw rotates it moves material through the instrument and causes it to melt and transition to a fluid-like phase, allowing for light mixing. SSE is still widely used today as an industry standard, mostly for physical processing (shaping) of polymeric products.

Twin screw extrusion (TSE) methodology followed the rapid growth of plastic materials in the 20th Century, and was first patented by Roberto Colombo in 1939 [15, 16, 18]. Twin screw extrusion is a more intense method of plastics processing, and uses two

rotating screws within a stationary barrel, rather than one [15-18]. Figure 2.1.2 illustrates the major differences between SSE and TSE.

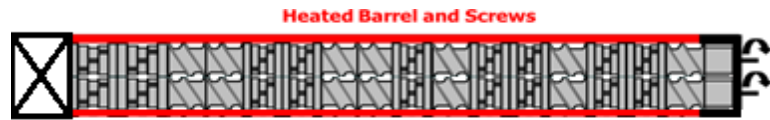


Figure 2.1.2: Typical twin screw extrusion setup (top-view)

One main difference between TSE and SSE is that TSE uses two screws; consequently, TSE contains a screw-to-screw intermeshed zone. This zone has a higher mixing capability than the screw-barrel contact zone found in SSE. A second difference is screw type; TSE employs both helical conveying screws and bilobe kneading discs, whereas SSE employs only conveying elements. The kneading discs allow for very high shear to occur within TSE [15, 17, 20]. The combination of the intermeshed zone and kneading discs results in better blend dispersion, filler exfoliation in composites, and homogenization of mixtures [21-23].

Up until the 1990's, extrusion had been almost exclusively performed in the melt phase. Materials being processed would be heated above the melt or glass transition temperature, in order to allow for good mixing and uniform flow. Although very successful, melt extrusion suffers from some common issues such as incomplete mixing/dispersion, low blend quality (known as incompatibility), and thermal degradation [1, 24, 25]. In the mid-1990's, researchers at Northwestern University developed an alternative approach to plastics processing and chose to cool materials

during processing rather than heat them [1]. This method keeps material below its melt or glass transition temperature, and imparts high levels of shear and compression in the solid state.

Their process, called solid-state shear pulverization (SSSP), has been shown to produce certain materials that were difficult to manufacture using TSE [5, 6, 9, 12-14, 26, 27]. Figure 2.1.3 shows the setup of an SSSP machine.



Figure 2.1.3: Typical solid-state shear pulverization setup (top-view)

SSSP methodology is rather unique and novel, and is only practiced at Northwestern University and Bucknell University. The process is geometrically identical to TSE and the two methods *only* differ in process temperatures (hot for TSE and cold for SSSP); however, there are significant consequences of this difference. Material processed via SSSP is in the solid state, and is therefore subjected to high impact and shear within the extruder. This intense action generates a significant amount of heat, which must be removed in order to keep the process material solid. The barrels of the extruder are thus cooled rather than heated. Solid, powder or flake output is produced in SSSP, in contrast to molten extrudate in TSE. Because of the significantly higher impact and shear levels in the solid state, SSSP is more effective than TSE at blending immiscible polymer systems and exfoliating fillers within composites [6, 9, 24, 25].

2.2 Instrumentation

Bucknell University uses a KraussMaffei Berstorff ZE-25 UTX laboratory-scale extruder, shown in Figure 2.2.1, for both TSE and SSSP operation.



Figure 2.2.1: The KraussMaffei Berstorff ZE-25 UTX extruder at Bucknell University

The size of the extruder is typically expressed by the “length over diameter” (L/D) ratio, as well as the screw diameter. Under TSE operation the L/D ratio is 34, while under SSSP operation the L/D ratio is 36. The diameter of each screw is 25 mm for both TSE and SSSP cases. By design, this extruder is a co-rotating and self-wiping machine. This means that the screws rotate in the same direction and are intermeshed. Figure 2.2.2 shows co- vs. counter-rotating and intermeshed vs. non-intermeshed (or tangential) designs.

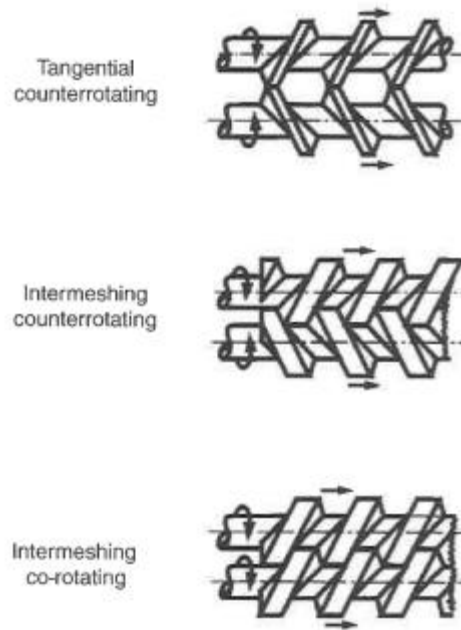


Figure 2.2.2: Various classifications of twin screw machines [17]

The co-rotating and intermeshed screws in the extruder are composed of a number of individual modular elements that can be configured in a variety of ways. Two major types of elements are used in the design of a typical SSSP screw. Conveying elements, as seen in Figure 2.2.3, are helical in shape, and are designed to quickly push material down the barrel of the extruder. They do not impart large forces to the material. Conveying elements can be thought of as a single long channel wrapped around a cylindrical rod. Material travels through this channel, spinning around the rod and moving down the barrel.



Figure 2.2.3: From left to right; small, medium, and large conveying elements used in Bucknell's SSSP machine

Kneading elements are designed to impart large mechanical energy to process material in SSSP. In TSE these elements are designed for intense mixing via stretch and flow (thus kneading), but in SSSP the elements are used to pulverize and grind the polymer. There is no pitched flight in a kneading element that forces a forward flow (as is the case for conveying elements). Instead, kneading elements are constructed from repeated and staggered bilobe discs, as can be seen in Figure 2.2.4. The orientation of the discs is designed to instigate forward, neutral, or reverse flow.



Figure 2.2.4: Kneading elements used in Bucknell's SSSP machine; from left to right, small forward, small neutral, small reverse, large forward

The barrels of the extruder are also modular, and have two intermeshed 25mm diameter channels for the material to travel through, as seen in Figure 2.2.5.



Figure 2.2.5: Cross section of the ZE-25 extruder barrels

There are 6 total zones, corresponding to the 6 serial modular barrels, in the extruder, and each can be set to a different temperature during operation. Bucknell's extruder circulates an ethylene glycol-water mixture cooled to 11 °F (-12 °C) through the instrument. The coolant enters and coils around the intermeshed channels as shown in Figure 2.2.6, removing a significant amount of any heat that is generated.

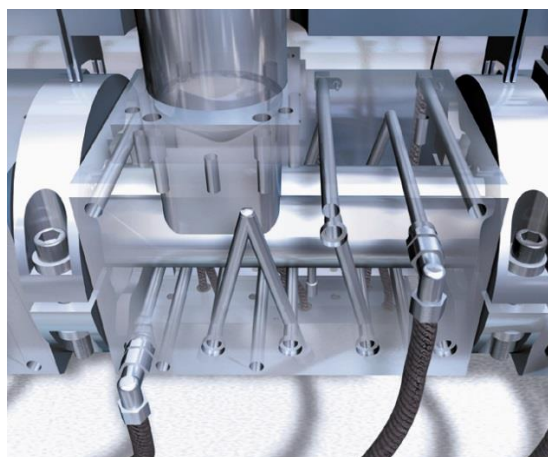


Figure 2.2.6: Location of the cooling lines in one of the modular barrels (zones) in the ZE-25 UTX extruder

Figure 2.2.6 shows the structure of a single zone of the extruder. Each zone can be assigned a setpoint temperature, and an onboard computer will circulate coolant and/or heat the zone as needed. Electrical induction cartridge-type heaters are used to heat the individual zones. The ZE-25 extruder is capable of controlling temperatures in the range of 11 °F (-12 °C) to higher than 600 °F (315 °C).

2.3 Heat Transfer within SSSP

The unique feature of the SSSP process is the intense grinding with high amounts of solid-state shearing done by the screws to the material. Raw materials, such as polymer pellets and powder fillers, are fed into the extruder and are subjected to repeated fragmentation and fusion. The intense physical pulverization and shear can then result in mechanochemical effects such as chain scission, chain branching, and compatibilization [2-14]. These physical and chemical effects can generate large amounts of heat, which is combated by SSSP's cooling system. However, the chiller system is not always able to remove all of the heat generated by the polymer during operation, and so under certain conditions a melt transition can occur. In the case of a melt transition, the process material becomes fluid-like, and the process becomes akin to TSE. The actual operating temperature in an SSSP operation is dependent on the interplay of the amount of heat generated by the material and the amount of heat pulled away by the coolant. Heat is generated by the flow of material in the form of friction and viscous dissipation, physical deformation of the polymer, and mechanochemical alteration of the polymer's molecular

structure. The balance of heating and cooling results in operating temperatures experienced by the powder as it flows through the extruder.

Temperature is a thermal property that describes how hot or cold a system is, and can be related to the energy streams flowing into and out of that given system. Energy flowing into a system will make it hotter, while energy flowing away will make it colder. If a boundary is placed around the extruder, the net sum of energy streams into and out of the system should be zero, based on the law of conservation of energy [26]. This is known as an energy balance, the standard form of which is shown as Eq. 2.3.1.

$$\text{Accumulation} = \text{Input} - \text{Output} + \text{Generation} \quad \text{Eq. 2.3.1}$$

Figure 2.3.1 was developed to describe SSSP in the form of a general, macroscale energy balance [11].

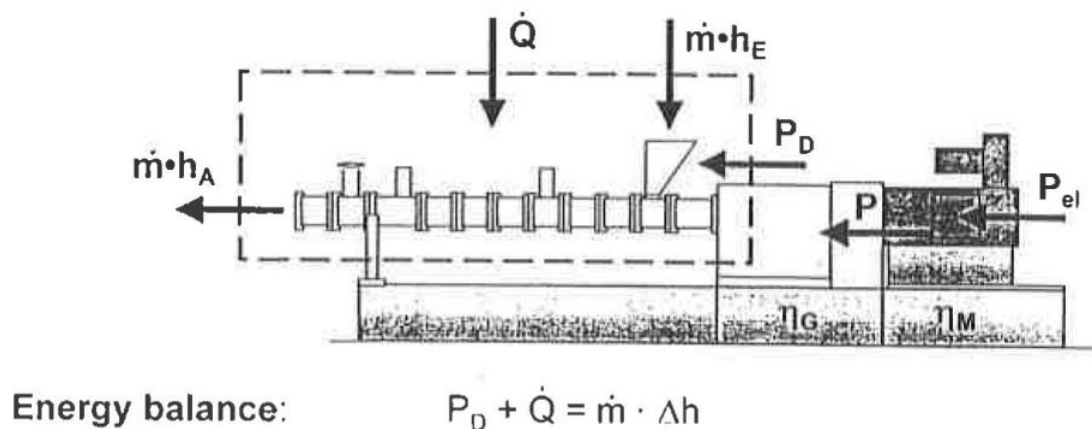


Figure 2.3.1: Overall, general energy balance for SSSP system [11]

The diagram in Figure 2.3.1 illustrates the major energy flows in SSSP. Arrows pointing into the boxed region indicate input streams, where arrows pointing out of the boxed

region signify output terms. In the case of steady state operation, there is no accumulation of energy within the system. The model developed by Khait et al. also does not consider generation of heat within SSSP. As a result, Eq. 2.3.1 simplifies to Eq. 2.3.2.

$$0 = Input - Output \quad \text{Eq. 2.3.2}$$

Eq. 2.3.2 can be more explicitly written by inserting the input and output streams as shown in Figure 2.3.1. Eq. 2.3.3 shows the net energy balance of SSSP.

$$0 = [\dot{Q} + \dot{m} \cdot h_E + P_D]_{input} - [\dot{m} \cdot h_A]_{output} \quad \text{Eq. 2.3.3}$$

\dot{Q} is the heat flux, \dot{m} is the mass flow rate, h_i is the enthalpy of either the incoming or outgoing material, and P_D is the motor power. The heat flux, \dot{Q} , is positive for TSE (i.e. heating of the barrels) and negative for SSSP (i.e. cooling of the barrels).

This simple model is useful in describing the flows of energy in the system and analyzing the amount of power needed to process a material. A rough approximation of process temperature can be derived from Eq. 2.3.3; however, it is not specific enough to describe the actual temperatures experienced by the material throughout the SSSP process. Eq. 2.3.3 draws a boundary around the entirety of the extruder, and does not pertain to individual zones or individual screw elements. Therefore, it is impossible to derive a temperature profile along the extruder from Eq. 2.3.3.

In practice, parameters that operators would control in an SSSP operation, such as screw speed, feed rate, and coolant temperature, have direct relations on the temperature profile. The intrinsic physical properties of the material being processed also dictate the temperature profile. These ideas have historically been understood qualitatively and have been based on experience and trial-and-error practices. Therefore, in order to quantify the

effect of different transport phenomena on the operation of SSSP, there is a need to model the temperature profile on a finer scale. As discussed above, the current general energy balance is insufficient for this task; Eq. 2.3.3 does not consider or “see” individual zones or screw elements. Rather than considering macroscopic energy flows such as P_D and \dot{Q} , SSSP can be modeled by considering transport phenomena in a single screw element; this corresponds to placing the boundaries of the balance around a single element. The laws of conservation of mass, conservation of momentum, and conservation of energy can be applied to generate functions that describe the dependence of system properties on time and space [28]. Chapter 3 lays out this modeling approach and describes its use in this thesis.

3. Problem Definition and Modeling Approach

3.1 Overarching Goals of the Thesis

This thesis aims at quantifying the effects of changing process parameters and varying material properties on process temperature, in an effort to develop a deeper understanding of heat transfer within SSSP. Detailed modeling by way of continuum mechanics would give insight into when and why a material would experience a melt transition during operation. In particular, the resulting modelling platform should be able to answer the following two questions.

1. What is the effect of processing and instrumentation parameters on the temperature profile and heat transfer?
 - Screw Rotation Speed
 - Feed Rate
 - Coolant Temperature
 - Set Temperature vs. Measured Temperature vs. Actual Temperature
2. What is the effect of material properties on the temperature profile and heat transfer?
 - Viscosity
 - Thermal Conductivity
 - Heat Capacity

This thesis approaches the above questions by modeling the system using the laws of conservation of mass, momentum, and energy, as discussed in the next section.

3.2. Modeling Technique

Transport phenomena deals with the conservation of mass, momentum, and energy, and is based on continuum mechanics. SSE and TSE have frequently been modeled using this approach [29-31]. Continuum mechanics describes a body and how the conserved quantities (mass, momentum, energy) are transported in/through that body over space and time. Figure 3.2.1 shows a body with arbitrary volume in two different configurations; a reference configuration and a deformed configuration.

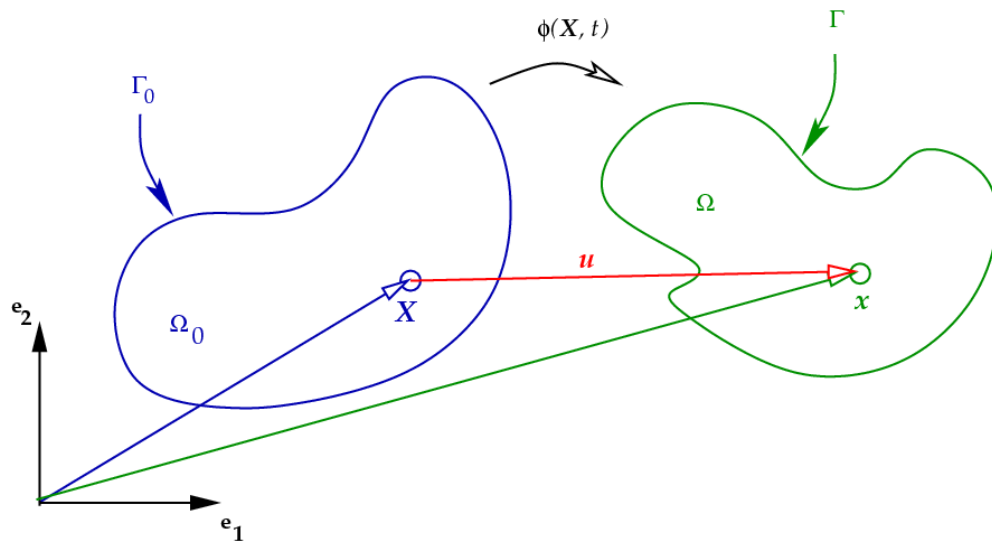


Figure 3.2.1: Representation of an arbitrary volume of material moving through space and time [32]

At $t = 0$ and position \vec{X} , the volume is at an initial reference state. Γ_0 and Ω_0 are the volume's reference boundary and reference configuration, respectively. As the volume moves with a velocity, \vec{u} , it changes its configuration by deforming its boundary and moving in space. The new boundary is written as Γ and the new configuration is written

as Ω . Furthermore, the new position can be described by a new position vector, \vec{x} .

Transforming from Γ_o and Ω_o to Γ and Ω is described by the function $\phi(\vec{X}, t)$. ϕ is useful in that it describes a given quantity in terms of space and time; this concept can be applied to SSSP and can be used to develop velocity and temperature profiles for the system.

Mass, momentum, and energy are always conserved in a given closed system and can be described using balance equations. Eqs. 3.2.1 – 3.2.3 are the differential balances on mass, momentum, and energy, respectively [28].

$$\frac{\partial \rho}{\partial t} + \nabla \cdot \rho \vec{v} = 0 \quad \text{Eq. 3.2.1}$$

$$\rho \frac{\partial \vec{v}}{\partial t} + \rho \vec{v} \cdot \nabla \vec{v} = -\nabla \vec{P} - \nabla \cdot \boldsymbol{\tau} + \rho \vec{g} \quad \text{Eq. 3.2.2}$$

$$\rho \frac{D\vec{v}}{Dt} = -\nabla \cdot \vec{q} - P(\nabla \cdot \vec{v}) - \boldsymbol{\tau} : \nabla \vec{v} \quad \text{Eq. 3.3.3}$$

Eq. 3.2.1 balances the accumulation of mass in a specific volume with the flow of mass through that volume; it is known as the equation of continuity. Eq. 3.2.2 is the equation of momentum and is a momentum balance on a given volume. It balances accumulation of momentum with inertia, stress, and external body forces. Eq. 3.2.3 is an energy balance and is known as the equation of energy. It considers convection, conduction, and generation of energy in a given volume. These three equations can be applied to any system and will always hold. Thus, they are powerful tools for describing a variety of physical systems. These equations are never solved outright; they are simplified and

reduced to more accessible equations through the use of various techniques, constraints, and assumptions that are specific to the system being described [28-31, 33]. In the context of SSSP, the equation of continuity and equation of momentum are used to develop a function for velocity in a screw channel. This velocity profile is then inserted into the equation of energy and is used to develop a temperature profile that can be used to analyze SSSP. The modeling specificities will be introduced and discussed in detail in Chapters 4 and 5.

The balance equations consider scalar, vector, and tensor quantities. A scalar quantity, such as temperature, is described by a single number; it has only a magnitude and no inherent direction in space or time. In this thesis, scalar quantities are represented by a non-bold letter, such as μ for viscosity. A vector is a collection of components, and indicates a magnitude and a direction. Vectors are represented as a non-bold letter with an arrow above, such as \vec{v} for velocity. A tensor is an object that describes higher order quantities within an object, such as stress within a solid. Tensors are shown as bold-faced letters, such as $\boldsymbol{\tau}$. An in depth explanation of scalars, vectors, tensors, and their related operations can be found in Appendix A of Transport Phenomena: Revised 2nd ed., by Bird, Stewart, and Lightfoot [28].

Heat transfer within twin screw extruders has been thoroughly explored and modeled through the late 1900's, and numerous researchers have produced models for velocity and temperature profiles within an extruder [30, 31, 33, 34] using Eqs. 3.2.1 – 3.2.3. Although many of these models exist, they are for melt extrusion processes and are not directly applicable to SSSP. This thesis aims at adopting the approaches used to

model TSE in order to apply them to SSSP. Chapter 4 discusses the specific geometry of the screw elements and develops velocity profiles for SSSP. Chapter 5 uses these velocity profiles to develop temperature profiles.

4. Development of Velocity Profiles

This section of the thesis develops the profiles of velocity for conveying and kneading elements. The balances and methodology presented in Chapter 3 are applied and simplified to determine the differential equations responsible for describing flow in the extruder. Assumptions are made to simplify the balances, and include no-slip, incompressible flow, and several scaling arguments. Boundary conditions are applied to produce the explicit profile for velocity in the screw channel region.

4.1 Conveying Elements

In SSSP, the conveying elements are responsible for transporting material down the barrel and through the extruder. These elements are helical in shape, and move material by dragging it forward with their pitched flights. The development in this section applies the equations of continuity and momentum to the specific geometry of a conveying element, and proposes a velocity profile that describes the flow of material through it.

To begin, the geometry of the screw must be described in detail. Figure 4.1.1 is an image of the three conveying elements used in this study.



Figure 4.1.1: From left to right: small, medium, and large conveying elements used in Bucknell's SSSP machine

In practice, the elements are placed on a rotating rod (i.e. a cylinder), and thus cylindrical coordinates may be a default coordinate system to employ, as seen in Figure 4.1.2a; the r -direction is perpendicular to the axis of screw rotation, the θ -direction moves with the rotation of the screw, and the z -direction is parallel to the axis of screw rotation. However, as shown further in Figure 4.1.2a and in Figure 4.1.2b, we choose Cartesian coordinates instead, by “unwinding” the element in the direction of the screw channel, based on previous work with TSEs [1,2]. Unwinding the helical screw converts the flow to a linear channel flow.

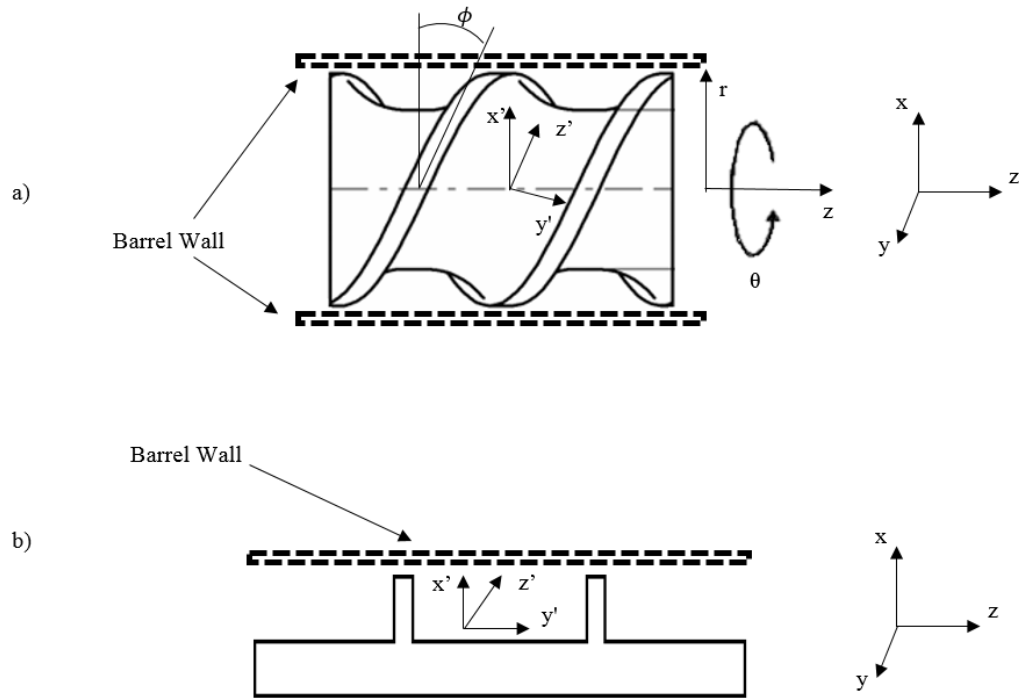


Figure 4.1.2: (a) Screw element with cylindrical and Cartesian coordinates and (b) “unwound” screw with Cartesian coordinates

The x' -direction is along the channel height, and corresponds to the r -direction. The y' -direction is perpendicular to the helical channel, and the z' -direction is parallel to the helical channel. As can be seen, the Cartesian coordinate system used to describe conveying elements is tilted at an angle equal to the complimentary angle of the flight angle, ϕ . As seen in Figure 4.1.1, conveying elements have three different sub-types; small ($\phi = 13.43^\circ$), medium ($\phi = 17.66^\circ$), and large ($\phi = 21.70^\circ$). Because the flight angles differ for each of these elements, three different coordinate systems are generated. In the development of the velocity and temperature profiles of the whole screw, these three different “tilts” in individual screw element will be remapped to a non-tilted coordinate system.

The direction of material flow is aligned with the positive z' -direction. The Cartesian coordinates used in this section are all labeled with a prime symbol as a reminder of the tilt in the coordinate system relative to the non-prime system. The prime symbol indicates a rotation of the coordinate system about the x -axis, such that the x - and x' -directions are identical. The rotation is in the counter-clockwise direction around the x -axis by the angle that is complimentary to the flight angle.

Based on the unwound Cartesian coordinates, the rotating screw transforms into a simple parallel plate flow. Fixing these conditions to the screw, the screw is seen to be stationary while the barrel moves with a velocity equal and opposite to the tangential velocity of the screw. In other words, the *barrel* moves and pulls material in the positive z' direction.

Recalling that the instrument is a co-rotating, intermeshing twin-screw extruder, there are two flow regimes, shown in Figure 4.1.3.

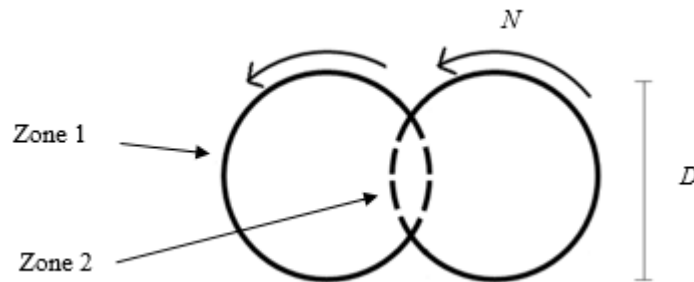


Figure 4.1.3: Cross-sectional view of intermeshed co-rotating twin-screws: solid line indicates Zone 1, or screw-barrel region; dotted line indicates Zone 2, or screw-screw region. D is the diameter of a single screw, N is the rotation rate of the screws.

Zone 1 in Figure 4.1.3 is the screw-barrel zone; again, the barrel is in motion and the screw is stationary. Zone 2 is the intermeshed screw-screw zone; here, based on the

reference frame of one of the screws, the opposite screw moves at a speed twice that of the tangential velocity of the screw. This is because the screws each move at the same velocity, but move in opposite directions in the intermeshed region. Figure 4.1.4 visualizes parallel plate flow in the two zones of a conveying element.

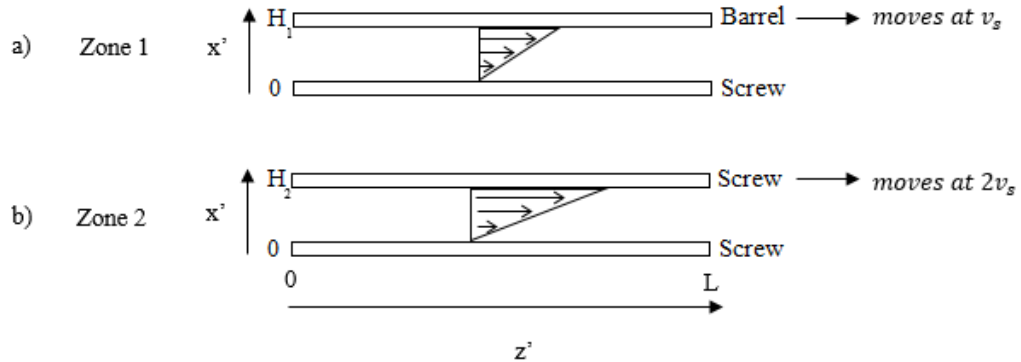


Figure 4.1.4: Representation of parallel plate flow in an unwound SSSP conveying element for (a) Zone 1, screw-barrel region and (b) Zone 2, intermeshed screw-screw region.

In Figure 4.1.4, the x' -direction extends from 0 to channel height, H ; the z' -direction extends from 0 to channel length, L . The top plate, in this scenario, moves at the screw's tangential velocity, v_s .

To develop the velocity profile, we first begin with the equation of continuity (EOC). From Equation 3.2.1, the EOC is applied as a balance of mass on the flow of material through a single element channel. Incompressibility states that the density of a material does not change as it flows. Water is considered an incompressible fluid, as are polymer melts. Seeing as these two types of fluids are considered incompressible, it follows that a flow of solid material in SSSP is incompressible as well. Therefore, Eq. 3.2.1 can be simplified to Eq. 4.1.1.

$$(\nabla \cdot \vec{v}) = \frac{\partial v_{x'}}{\partial x'} + \frac{\partial v_{y'}}{\partial y'} + \frac{\partial v_{z'}}{\partial z'} = 0 \quad \text{Eq. 4.1.1}$$

In general, \vec{v} is the velocity field of material in the screw flight, and can be expanded as shown in Eq. 4.1.2.

$$\vec{v} = v_{x'}(x', y', z', t)\vec{e}_{x'} + v_{y'}(x', y', z', t)\vec{e}_{y'} + v_{z'}(x', y', z', t)\vec{e}_{z'} \quad \text{Eq. 4.1.2}$$

Each coordinate direction is associated with a component of the field, and each of these components is a function of space and time. We continue by defining the following scale variables, which are used to non-dimensionalize the system.

$$\omega' = \frac{y'}{W} \quad \text{Eq. 4.1.3a}$$

$$\xi' = \frac{x'}{H} \quad \text{Eq. 4.1.3b}$$

$$\zeta' = \frac{z'}{L} \quad \text{Eq. 4.1.3c}$$

$$U_j = \frac{v_{ij}}{V_i} \text{ for } i = x', y', z' \text{ and } j = \xi', \omega', \zeta' \quad \text{Eq. 4.1.3d}$$

where W is the width of the channel, H is the height of the channel, L is the length of the channel, and V_i is an arbitrary scale velocity. Applying Eqs. 4.1.3a – 4.1.3d to Eq. 4.1.1 gives

$$\frac{v_{x'}}{H} \frac{\partial U_{\xi'}}{\partial \xi'} + \frac{v_{y'}}{W} \frac{\partial U_{\omega'}}{\partial \omega'} + \frac{v_{z'}}{L} \frac{\partial U_{\zeta'}}{\partial \zeta'} = 0 \quad \text{Eq. 4.1.4}$$

Equation 4.1.4 can be further reduced by comparing the coefficient of each term. With rearrangement, we find

$$V_{x'} \sim V_{z'} \frac{H}{L} \quad \text{Eq. 4.1.5}$$

$$V_{y'} \sim V_{z'} \frac{W}{L} \quad \text{Eq. 4.1.6}$$

Assuming that the screw channel length, L , is much larger than the channel height, H , and channel width, W , it follows that flows in the x' - and y' -directions can be ignored. That is to say, flows in the x' - and y' -directions are assumed to be insignificant when compared to flow in z' , because we assume $L \gg W, H$. Therefore, the only component of the velocity field is in z' .

$$\vec{v} = v_{z'}(x', y', z', t)\vec{e}_{z'} \quad \text{Eq. 4.1.7}$$

Neglecting the flows in x' - and y' -directions reduces Eq. 4.1.1 to

$$\frac{\partial v_{z'}}{\partial z'} = 0 \quad \text{Eq. 4.1.8}$$

Eq. 4.1.8 states that the velocity in the z' -direction is not a function of the z' -direction.

Applying the assumption of steady state along with Eq. 4.1.8 to Eq. 4.1.7 gives

$$\vec{v} = v_{z'}(x', y')\vec{e}_{z'} \quad \text{Eq. 4.1.9}$$

The equation of momentum, shown as Eq. 3.2.2, can now be simplified to describe flow in a conveying element channel. The z' -component of the equation of momentum for an incompressible, Newtonian fluid can be written as shown by Eq. 4.1.10. Although a Newtonian model does not completely describe the flow of material in the extruder, it does serve as a useful first approximation [35].

$$\rho \left(\frac{\partial v_{z'}}{\partial t} + v_{x'} \frac{\partial v_{z'}}{\partial x'} + v_{y'} \frac{\partial v_{z'}}{\partial y'} + v_{z'} \frac{\partial v_{z'}}{\partial z'} \right) = - \frac{\partial P}{\partial z'} + \mu \left[\frac{\partial^2 v_{z'}}{\partial x'^2} + \frac{\partial^2 v_{z'}}{\partial y'^2} + \frac{\partial^2 v_{z'}}{\partial z'^2} \right] + \rho g_{z'} \quad \text{Eq. 4.1.10}$$

Reapplying the assumption of steady state and considering Eqs. 4.1.8 and 4.1.9, Eq. 4.1.10 can be simplified to Eq. 4.1.11.

$$\frac{\partial P}{\partial z'} = \mu \left[\frac{\partial^2 v_{z'}}{\partial x'^2} + \frac{\partial^2 v_{z'}}{\partial y'^2} \right] \quad \text{Eq. 4.1.11}$$

Eq. 4.1.11 can be simplified further, and a more accessible velocity profile can be developed. Eq. 4.1.11 can be non-dimensionalized through x' , y' , z' , P , and $v_{z'}$, and subsequently simplified via the use of various scale factors. Eqs. 4.1.3a – 4.1.3d show the scale variables for x' , y' , z' , and $v_{z'}$. The scale variable for P is written as

$$\Gamma = \frac{P}{P_o} \quad \text{Eq. 4.1.12}$$

where P_o is an arbitrary scale pressure. Using Eqs. 4.1.3a – 4.1.3d with Eq. 4.1.12, Eq. 4.1.11 becomes Eq. 4.1.13.

$$\frac{P_o}{\mu L} \frac{\partial \Gamma}{\partial \zeta'} = \frac{v_o}{H^2} \frac{\partial^2 U}{\partial \xi'^2} + \frac{v_o}{W^2} \frac{\partial^2 U}{\partial \omega^2} \quad \text{Eq. 4.1.13}$$

Rearranging gives

$$\frac{P_o}{\mu L} \frac{\partial \Gamma}{\partial \zeta'} = \frac{v_o}{H^2} \left(\frac{\partial^2 U}{\partial \xi'^2} + \frac{H^2}{W^2} \frac{\partial^2 U}{\partial \omega^2} \right) \quad \text{Eq. 4.1.14}$$

Again considering the geometry of an individual screw, the width of the channel, W , is much larger than the height of the channel, and so $\frac{H}{W} \ll 1$. Thus $L \gg W \gg H$ is the basis of this analysis. Therefore, the last term in Eq. 4.1.14 can be dropped, giving

$$\frac{P_o}{\mu L} \frac{\partial \Gamma}{\partial \zeta'} = \frac{v_o}{H^2} \frac{\partial^2 U}{\partial \xi'^2} \quad \text{Eq. 4.1.15}$$

Reintroducing the definitions of Eqs. 4.1.3a – 4.1.3d and 4.1.12 back into Eq. 4.1.15 gives

$$\frac{dP}{dz'} = \mu \frac{d^2 v_{z'}}{dx'^2} \quad \text{Eq. 4.1.16}$$

Eq. 4.1.16 is a differential equation that describes the pressure-dependent, drag flow of material in the screw channel. Revisiting Eq. 4.1.8, $v_{z'}$ is not dependent on z' , and

Eq. 4.1.16 is therefore separable in z' . Integrating through from P_o to P_L and from L_o to L_1 , gives

$$\frac{\Delta P}{\Delta L} = \mu \frac{d^2 v_{z'}}{dx'^2} \quad \text{Eq. 4.1.17}$$

where ΔP is the change in pressure across a section of channel length ΔL . L is dependent on the type of screw element being considered. Eq. 4.1.17 is now a linear, differential equation, and has the following general solution.

$$v_{z'}(x') = \frac{\Delta P}{\mu \Delta L} \frac{x'^2}{2} + c_1 x' + c_2 \quad \text{Eq. 4.1.18}$$

Eq. 4.1.18 applies for flow within a conveying element screw channel, but must now be solved for two distinct zones; one full rotation of the screw passes through a barrel-screw contact zone (Zone 1) and an intermeshed screw-screw contact zone (Zone 2). Figure 4.1.4 shows schematic representations of the boundary conditions that can be used to determine an exact solution for Zones 1 and 2 from Eq. 4.1.18. The boundary conditions can be written as follows for Zones 1.

$$v_{z',1}(x = 0) = 0 \quad \text{Eq. 4.1.19a}$$

$$v_{z',1}(x = H_1) = v_s \quad \text{Eq. 4.1.19b}$$

Eqs. 4.1.19a and 4.1.19b apply to the screw-barrel contact region and are labeled with subscript 1. The tangential screw velocity, v_s , is

$$v_s = \pi D N \cos \phi \quad \text{Eq. 4.1.20}$$

This expression corresponds to the linear velocity of the screw at its outermost edge (i.e. the base of the channel). Figure 4.1.5 shows the full unwound surface of a single screw element through one rotation.

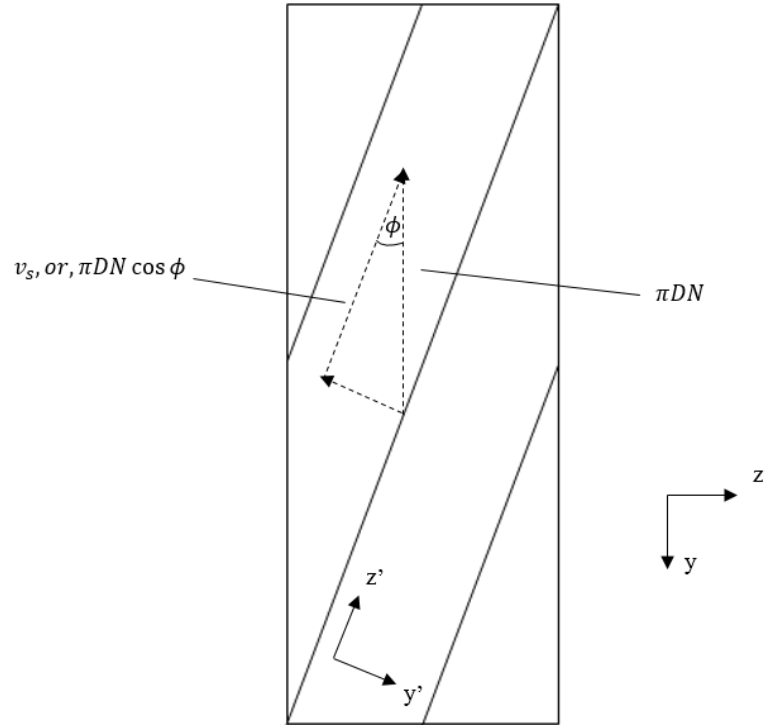


Figure 4.1.5: Flattened surface of a conveying element; diagonal lines represent the flights. The dashed arrows represent the velocity of the barrel in the negative y -direction and its components in the positive y' - and z' -directions.

D is the diameter of the screw, N is the rotation rate of the screw, and ϕ is the angle of the screw flights. The $\cos \phi$ term accounts for the “tilt” in the coordinate system.

Applying the Zone 1 boundary conditions to general solution, the velocity profile of material travelling through Zone 1 is found as

$$v_{z',1}(x') = v_s \frac{x'}{H_1} - \frac{\Delta P_1}{\mu \Delta L_1} \frac{H_1^2}{2} \left(\frac{x'}{H_1} - \frac{x'^2}{H_1^2} \right) \quad \text{Eq. 4.1.21}$$

Eq. 4.1.21 describes the flow of material through the extruder as a balance between drag flow and pressure flow. The first term on the right hand side characterizes drag effects and the second term on the right hand side characterizes pressure effects. In the case of

zero pressure rise or drop, the profile is purely drag flow and is linear. Increasing effects of pressure lead to a parabolic shape of the velocity profile.

The boundary conditions can be written as follows for Zone 2.

$$v_{z',2}(x = 0) = 0 \quad \text{Eq. 4.1.22a}$$

$$v_{z',2}(x = H_2) = 2v_s \quad \text{Eq. 4.1.22b}$$

Eqs. 4.1.22a and 4.1.22b apply to the screw-screw contact region and are labeled with a subscript 2. Applying the Zone 2 boundary conditions to the general solution gives

$$v_{z',2}(x') = 2v_s \frac{x'}{H_2} - \frac{\Delta P_2 H_2^2}{\mu \Delta L_2} \frac{1}{2} \left(\frac{x'}{H_2} - \frac{x'^2}{H_2^2} \right) \quad \text{Eq. 4.1.23}$$

These results are of similar form to velocity profiles in literature [34]. Eq. 4.1.23 is almost identical to Eq. 4.1.21, with the exception of the drag term. The drag effects in Zone 2 are larger than those in Zone 1 due to the competing motion of the intermeshed screws. These two velocity profiles are valid for two different zones in the screw.

Moving forward, it would be convenient to collapse the two individual zone profiles into a single effective profile through appropriate approximations. In the operation of an SSSP instrument, the conveying elements are frequently starve fed. This means that material is fed at a flow rate such that the volume of the channel is never fully filled. As a result, pressure cannot develop, and the flow can be viewed as pure drag flow. Considering the specific case of zero pressure rise or drop, Eqs. 4.1.21 and 4.1.23 reduce to

$$v_{z',1}(x') = v_s \frac{x'}{H} \quad \text{Eq. 4.1.24}$$

$$v_{z',2}(x') = 2v_s \frac{x'}{H} \quad \text{Eq. 4.1.25}$$

Revisiting the two zone split, Figure 4.1.6 illustrates the two regions that are described by Eqs. 4.1.24 and 4.1.25.

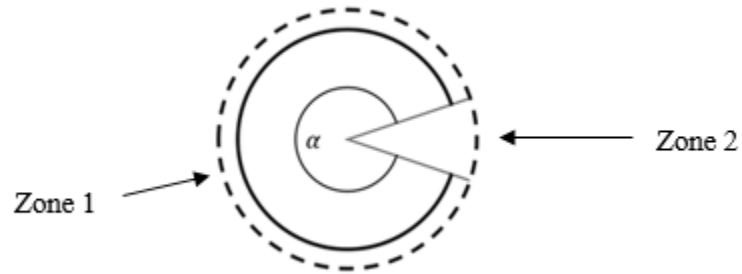


Figure 4.1.6: Cross section of one of the twin-screws, showing Zones 1 and 2

One full rotation of the screws occurs through the angle 2π . We define a fraction of the rotation as

$$\varphi = \frac{\alpha}{2\pi} \quad \text{Eq. 4.1.26}$$

Therefore, for the fraction φ the material is in Zone 1, and for the fraction $1 - \varphi$ the material is in Zone 2.

If the screw is unwound, Figure 4.1.6 can be transformed into Figure 4.1.7.

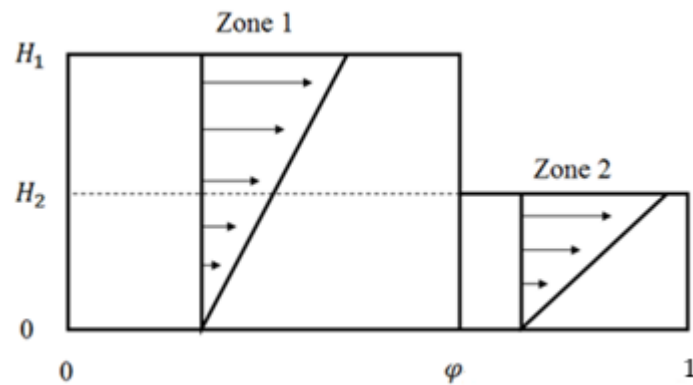


Figure 4.1.7: Unwound screw representation of the two flow regions in a conveying element

Figure 4.1.7 shows that as material moves from Zone 1 to Zone 2, there is a change in channel height. When comparing Eqs. 4.1.21 and 4.1.23, it is also apparent that the effects of drag increase in Zone 2, leading to a higher shear rate.

We define H_t as the average height of the channel through a single rotation. This average height can be expressed as

$$H_t = \varphi H_1 + (1 - \varphi)H_2 \quad \text{Eq. 4.1.27}$$

which is simply a weighted average of the heights in each zone.

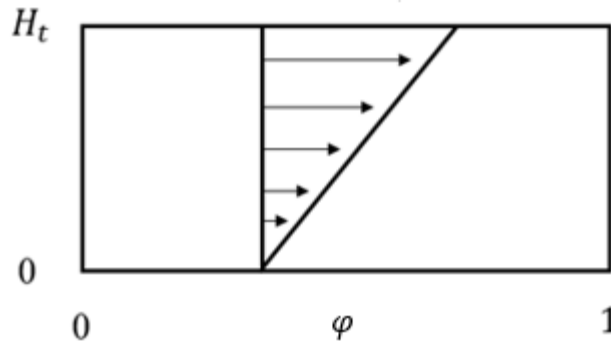


Figure 4.1.8: Representation of the effective velocity profile, v_t , of Zones 1 and 2 through a full rotation

The length of this effective zone is the sum of the individual lengths of Zone 1 and Zone 2; it is the length of one full rotation. $v_{z',1}$ is only defined in Zone 1 and $v_{z',2}$ is only defined in Zone 2. The proposed averaged height can be used to define an alternative *effective* profile.

This effective profile can be defined through the application of the equation of continuity, which requires that mass flowing through Zones 1 and 2 be conserved.

$$\dot{m}_1 = \dot{m}_2 = \dot{m}_t \quad \text{Eq. 4.1.28}$$

Reapplying the assumption of incompressible flow gives

$$\dot{v}_1 = \dot{v}_2 = \dot{v}_t \quad \text{Eq. 4.1.29}$$

where \dot{v}_i is the volumetric flow rate through a given zone. The volumetric flow rate can be reduced to

$$\langle v_{z',1} \rangle WH_1 = \langle v_{z',2} \rangle WH_2 = \langle v_t \rangle WH_t \quad \text{Eq. 4.1.30}$$

The width of the channel in each zone remains constant, giving

$$\langle v_{z',1} \rangle H_1 = \langle v_{z',2} \rangle H_2 = \langle v_t \rangle H_t \quad \text{Eq. 4.1.31}$$

with the *average* channel velocity for a given zone defined by

$$\langle v_i \rangle = \frac{1}{H_i} \int_0^{H_i} v_i(x') dx' \quad \text{Eq. 4.1.32}$$

Eq. 4.1.31 gives the averaged effective velocity profile as a function of either the averaged Zone 1 velocity profile or the averaged Zone 2 velocity profile. In the case of conveying elements, where velocity profiles are linear, Eq. 4.1.32 allows us to write

$$\langle v_{z',1} \rangle = \frac{v_s}{2} \quad \text{Eq. 4.1.33}$$

$$\langle v_{z',2} \rangle = v_s \quad \text{Eq. 4.1.34}$$

Eqs. 4.1.32 and 4.1.33 thus give the result that $\langle v_{z',2} \rangle = 2\langle v_{z',1} \rangle$ for the specific case of no pressure development in conveying elements. Using this result and Eq. 4.1.34 gives

$$\langle v_{z',1} \rangle H_1 = 2\langle v_{z',1} \rangle H_2 \quad \text{Eq. 4.1.35}$$

Eq. 4.1.35 can then be reduced to the following.

$$H_1 = 2H_2 \quad \text{Eq. 4.1.36}$$

Eq. 4.1.36 provides a metric which we can appropriately apply to Eq. 4.1.31. It says that if the height of Zone 1 is twice that of Zone 2, then the averaged effective profile can be

calculated from either $\langle v_{z',1} \rangle$ or $\langle v_{z',2} \rangle$, with no difference between the results. For the case of Bucknell's conveying elements, the Zone 1 channel height is approximately twice that of the Zone 2 height, fulfilling the condition prescribed by Eq. 4.1.36 (Zone 1 channel height = ~4 mm and Zone 2 channel height = ~2 mm).

Continuing with this development, we use Eq. 4.1.32 to calculate the averaged effective velocity profile from the averaged Zone 1 profile, as follows.

$$\langle v_t \rangle = \frac{\langle v_{z',1} \rangle H_1}{H_t} = \frac{v_s H_1}{2H_t} \quad \text{Eq. 4.1.37}$$

Applying Eq. 4.1.36 to the definition of H_t gives

$$H_t = \frac{H_1}{2} (1 + \varphi) \quad \text{Eq. 4.1.38}$$

Inserting Eq. 4.1.38 into the right hand side of Eq. 4.1.37 then gives

$$\langle v_t \rangle = \frac{v_s}{(1+\varphi)} \quad \text{Eq. 4.1.39}$$

Eq. 4.1.39 is also the result of starting the calculation for $\langle v_t \rangle$ with $\langle v_{z',2} \rangle$. If the form of the effective velocity profile $v_t(x')$ is assumed to be of the same form as $v_{z',1}(x')$ and $v_{z',2}(x')$, then it follows that

$$v_t(x') = \frac{2v_s}{(1+\varphi)} \frac{x'}{H} \quad \text{Eq. 4.1.40}$$

Eq. 4.1.43 is linear, indicating that the flow is purely drag-induced; this is specifically valid only for the case of no pressure rise/drop in conveying elements. It is an *effective* profile that is derived from the application of conservation of mass to Zones 1 and 2, along with the definition of an average channel height, H_t . Figure 4.1.9 shows the general shape of conveying drag profiles.

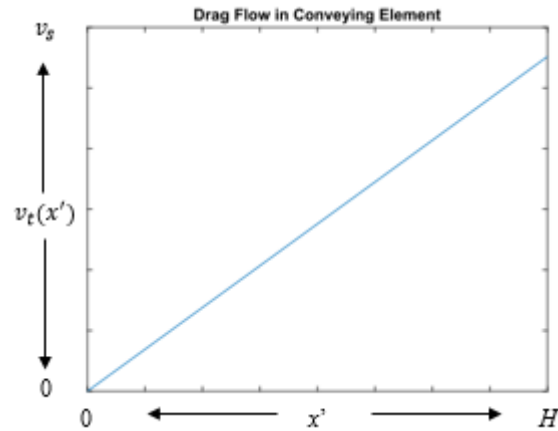


Figure 4.1.9: Shape of the effective conveying velocity profile

In preparation for Chapter 5, we redefine the dimensionless velocity as

$$U(\xi) = \frac{v_t(x')}{v_s} \quad \text{Eq. 4.1.41}$$

Applying Eq. 4.1.41 and the scale variable ξ' to Eq. 4.1.40 gives

$$U(\xi') = \frac{2\xi'}{(1+\varphi)} \quad \text{Eq. 4.1.42}$$

4.2 Kneading Elements

Kneading elements differ from conveying elements in that they are not built with the sole purpose of transporting material through the machine. These elements are more specialized, focusing on pulverizing and shearing the material. In that spirit, they are not pitched like conveying elements; the discs that make up kneading elements are more jagged, and are fully intermeshed. Figure 4.2.1 shows the various kneading elements used in this study:

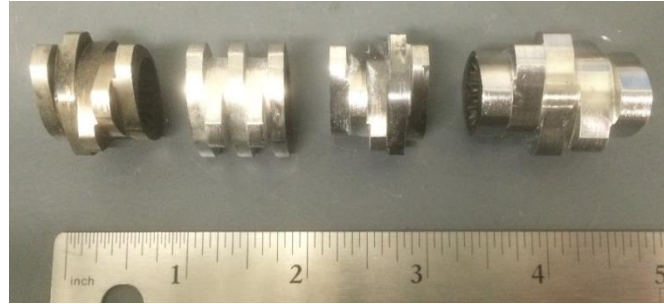


Figure 4.2.1: Kneading elements used in Bucknell's SSSP machine; from left to right, small forward, small neutral, small reverse, large forward

Contrary to the development of conveying elements, cylindrical coordinates are used to describe flow in kneading elements. This is done because the kneading element-barrel system can be approximated as two concentric cylinders. Figure 4.2.2 shows the relationship between the screw element and the cylindrical coordinate system.

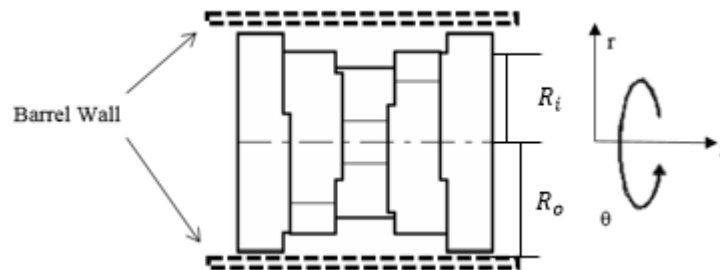


Figure 4.2.2: Illustration of the cylindrical coordinate system assigned to kneading elements

Material flows in the positive z -direction, and is simultaneously sheared in the θ -direction. As the screw rotates within the barrel of radius R_o , the low edges of the bilobe discs effectively form an inner radius, R_i , where the material flows in the gap between R_i and R_o . Figure 4.2.3 shows a cross-sectional view of a single screw element.

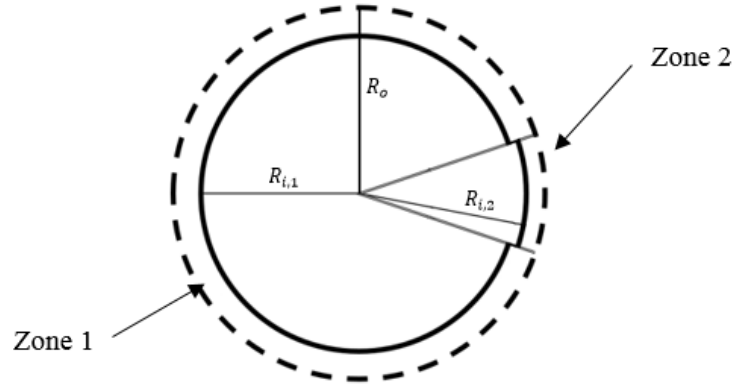


Figure 4.2.3: Axial view of the “smoothed” kneading element-barrel system; Zone 1 is the screw-barrel region, and Zone 2 is the screw-screw region

The two zone concept still applies here, where Zone 1 is the screw-barrel region and Zone 2 is the screw-screw region. The inner radius R_i is larger for Zone 2 than Zone 1, corresponding to smaller gap in Zone 2 than in Zone 1. The inner radius for Zone 1 can be written as $R_{i,1}$ and for Zone 2 as $R_{i,2}$. The outer radius R_o is the same for both Zones 1 and 2. The following equations define the ratios κ_i [28].

$$\kappa_1 = \frac{R_{i,1}}{R_o} \quad \text{Eq. 4.2.1}$$

$$\kappa_2 = \frac{R_{i,2}}{R_o} \quad \text{Eq. 4.2.2}$$

These ratios allow us to define the inner radii as functions of the outer radii, given that we know the values of κ_i . Eqs. 4.2.1 and 4.2.2 allow for a cleaner representation of the velocity profiles.

As in the development of the conveying element velocity profiles, here we take the reference frame of the kneading screw element. As a result, the screw is stationary and the barrel moves at some angular velocity Ω_o . The starting point for this derivation

is, as with the conveying element development, the equation of continuity, Eq. 3.2.1. For an incompressible fluid, the cylindrical form of the equation of continuity is

$$(\nabla \cdot \vec{v}) = \frac{1}{r} \frac{\partial(rv_r)}{\partial r} + \frac{1}{r} \frac{\partial v_\theta}{\partial \theta} + \frac{\partial v_z}{\partial z} = 0 \quad \text{Eq. 4.2.3}$$

\vec{v} can be expanded into a more explicit representation of the flow field, shown as

$$\vec{v} = v_r(r, \theta, z, t)\vec{e}_r + v_\theta(r, \theta, z, t)\vec{e}_\theta + v_z(r, \theta, z, t)\vec{e}_z \quad \text{Eq. 4.2.4}$$

Bird et al. [28] discusses flow in a Couette viscometer, which considers the flow of material in concentric cylinders. The kneading element system is analogous to the Couette viscometer, with the addition of an axial flow. Following the approach given by Bird et al. [28, 36], we can assume that the velocity components are

$$v_r = 0 \quad \text{Eq. 4.2.5}$$

$$v_\theta = v_\theta(r) \quad \text{Eq. 4.2.6}$$

$$v_z = v_z(r) \quad \text{Eq. 4.2.7}$$

Eq. 4.2.4 thus reduces to

$$\vec{v} = v_\theta(r)\vec{e}_\theta + v_z(r)\vec{e}_z \quad \text{Eq. 4.2.8}$$

where flow in the θ - and z -directions are only dependent on r .

Applying Eq. 4.2.8 to Eq. 4.2.3 gives

$$\frac{1}{r} \frac{\partial v_\theta}{\partial \theta} + \frac{\partial v_z}{\partial z} = 0 \quad \text{Eq. 4.2.9}$$

Inserting Eqs. 4.2.6 and 4.2.7 into 4.2.9 shows that the equation of continuity holds, and mass is conserved. Moving forward, we now look at the equation of motion in cylindrical coordinates. According to Eq. 4.2.5, the r -component of the velocity field is zero, so only

the θ - and z -components of the equation of motion are considered. Eq. 3.2.2 is thus transformed into

$$\rho \left(\frac{\partial v_\theta}{\partial t} + v_r \frac{\partial v_\theta}{\partial r} + \frac{v_\theta}{r} \frac{\partial v_\theta}{\partial \theta} + v_z \frac{\partial v_\theta}{\partial z} + \frac{v_r v_\theta}{r} \right) = -\frac{1}{r} \frac{\partial P}{\partial \theta} + \mu \left[\frac{\partial}{\partial r} \left(\frac{1}{r} \frac{\partial}{\partial r} (r v_\theta) \right) + \frac{1}{r^2} \frac{\partial^2 v_\theta}{\partial \theta^2} + \frac{\partial^2 v_\theta}{\partial z^2} + \frac{2}{r^2} \frac{\partial v_r}{\partial \theta} \right] + \rho g_\theta \quad \text{Eq. 4.2.10}$$

$$\rho \left(\frac{\partial v_z}{\partial t} + v_r \frac{\partial v_z}{\partial r} + \frac{v_\theta}{r} \frac{\partial v_z}{\partial \theta} + v_z \frac{\partial v_z}{\partial z} \right) = -\frac{\partial P}{\partial z} + \mu \left[\frac{1}{r} \frac{\partial}{\partial r} \left(r \frac{\partial v_z}{\partial r} \right) + \frac{1}{r^2} \frac{\partial^2 v_z}{\partial \theta^2} + \frac{\partial^2 v_z}{\partial z^2} \right] + \rho g_z \quad \text{Eq. 4.2.11}$$

Considering the case of steady state flow, and applying Eqs. 4.2.5 and 4.2.6 to Eq. 4.2.10 gives

$$0 = \mu \frac{\partial}{\partial r} \left(\frac{1}{r} \frac{\partial}{\partial r} (r v_\theta) \right) \quad \text{Eq. 4.2.12}$$

Eq. 4.2.13 is valid for both Zones 1 and 2 in a kneading element, and has the following general solution.

$$v_\theta = \frac{c_1 r}{2} + \frac{c_2}{r} \quad \text{Eq. 4.2.13}$$

The boundary conditions on v_θ are dependent on the motion of the screw and barrel in θ . As stated above, the screw is considered stationary in this development, and the barrel moves at an angular velocity of Ω_o . As a result, the boundary conditions on v_θ for Zone 1 are

$$v_{\theta,1}(r = R_{i,1}) = 0 \quad \text{Eq. 4.2.14a}$$

$$v_{\theta,1}(r = R_o) = \Omega_o R_o \quad \text{Eq. 4.2.14b}$$

Applying the boundary conditions to the general solution gives the exact solution for v_θ in Zone 1 of the kneading elements, which can be written as

$$v_{\theta,1} = \frac{\Omega_o}{r} \left[\frac{(r^2 - R_{i,1}^2)}{(1 - \kappa_1^2)} \right] \quad \text{Eq. 4.2.15}$$

Eq. 4.2.15 suggests that flow for kneading elements in the θ -direction is purely a drag flow, with no effects of pressure.

For Zone 2, the boundary conditions are as follows.

$$v_{\theta,2}(r = R_{i,2}) = 0 \quad \text{Eq. 4.2.16a}$$

$$v_{\theta,2}(r = R_o) = 2\Omega_o R_o \quad \text{Eq. 4.2.16b}$$

The condition at $r = R_o$ for Zone 2 is twice that of Zone 1, as the screws are moving at the same angular velocity, yet in opposite directions. Applying the boundary conditions in Eqs. 4.2.16a and 4.2.16 to the general solution in Eq. 4.2.13 gives

$$v_{\theta,2} = \frac{2\Omega_o}{r} \left[\frac{(r^2 - R_{i,2}^2)}{(1 - \kappa_2^2)} \right] \quad \text{Eq. 4.2.17}$$

This result also suggests pure drag flow. The coefficient of 2 is a result of the intermeshed screws moving in equal and opposite directions. Figure 4.2.4 shows the general shape of these velocity profiles.

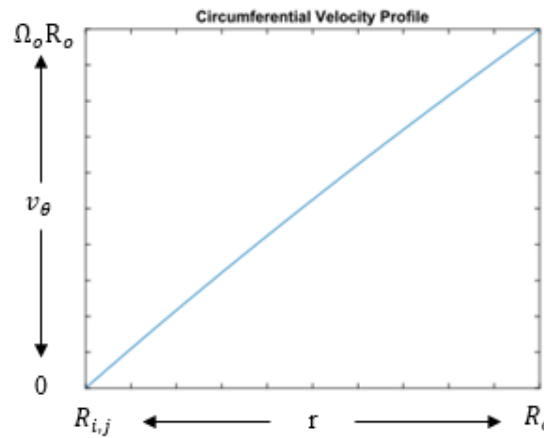


Figure 4.2.4: Circumferential velocity profile for kneading discs; $\Omega_o = 1 \text{ s}^{-1}$, $R_{i,j} = 10.5 \text{ mm}$, $\kappa_j = 0.84$

The circumferential profiles have a slight bend to them, and are not perfectly straight.

This is due to the dependence on $1/r$.

The profile of velocity in the z -direction can be similarly developed by applying Eqs. 4.2.5 and 4.2.7 to Eq. 4.2.11. Doing so gives

$$0 = -\frac{dP}{dz} + \frac{\mu}{r} \frac{\partial}{\partial r} \left(r \frac{\partial v_z}{\partial r} \right) \quad \text{Eq. 4.2.18}$$

In Eq. 4.2.18, μ and v_z are independent of z . Therefore, we can integrate Eq. 4.2.18 through z from L_0 to L_1 and through P from P_0 to P_1 to obtain the pressure drop, $\frac{\Delta P}{\Delta L}$,

where

$$\Delta P = P_1 - P_0 \quad \text{Eq. 4.2.19}$$

$$\Delta L = L_1 - L_0 \quad \text{Eq. 4.2.20}$$

After integration, Eq. 4.2.18 can be written as

$$\frac{\Delta P}{\Delta L} = \frac{\mu}{r} \frac{\partial}{\partial r} \left(r \frac{\partial v_z}{\partial r} \right) \quad \text{Eq. 4.2.21}$$

The general solution to Eq. 4.2.21 is written as

$$v_z = \frac{\Delta P}{\Delta L} \frac{r^2}{4\mu} + c_1 \ln(r) + c_2 \quad \text{Eq. 4.2.22}$$

The boundary conditions here depend on the motion of the screw and barrel surfaces in the z -direction instead of the θ -direction. The screw and barrel are both fixed in the z -direction, and are only free to move in the θ -direction. As a result, the boundary conditions on v_z for Zone 1 are homogeneous and written as

$$v_{z,1}(r = R_{i,1}) = 0 \quad \text{Eq. 4.2.23a}$$

$$v_{z,1}(r = R_o) = 0 \quad \text{Eq. 4.2.23b}$$

Applying the boundary conditions to Eq. 4.2.22 gives the exact solution for Zone 1, which is written as

$$v_{z,1} = -\frac{\Delta P_1 R_0^2}{\Delta L_1 4\mu} \left((1 - \kappa_1^2) \left[\frac{\ln\left(\frac{r}{R_0}\right)}{\ln(\kappa_1)} \right] - \left(1 - \frac{r^2}{R_0^2}\right) \right) \quad \text{Eq. 4.2.24}$$

The same set of boundary conditions can be applied to give the solution for Zone 2, instead considering $R_{i,2}$. This gives

$$v_{z,2} = -\frac{\Delta P_2 R_0^2}{\Delta L_2 4\mu} \left((1 - \kappa_2^2) \left[\frac{\ln\left(\frac{r}{R_0}\right)}{\ln(\kappa_2)} \right] - \left(1 - \frac{r^2}{R_0^2}\right) \right) \quad \text{Eq. 4.2.25}$$

Eqs. 4.2.24 and 4.2.25 thus represent the flow of material through the axial direction.

Figure 4.2.5 shows the shape of these profiles.

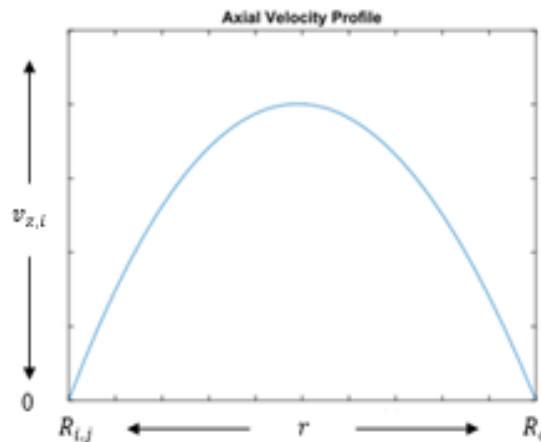


Figure 4.2.5: General shape of the axial pressure driven velocity profile in kneading elements; $\frac{\Delta P_j}{\Delta L_j} = 10 \text{ Pa/m}$, $R_o = 12.5 \text{ mm}$, $\kappa_j = 0.84$, $\mu = 1 \text{ Pa} \cdot \text{s}$

The axial flow in kneading elements is *only* pressure driven, and therefore is of a parabolic shape. Pressure drop must be negative in kneading elements in order to drive

forward flow. Material is sheared by the screw in the θ -direction, and driven by pressure gradients in the z -direction.

In summary, flow in kneading elements can be described by the following four equations.

$$v_{\theta,1} = \frac{\Omega_o}{r} \left[\frac{(r^2 - R_{i,1}^2)}{(1 - \kappa_1^2)} \right] \quad \text{Eq. 4.2.15}$$

$$v_{\theta,2} = \frac{2\Omega_o}{r} \left[\frac{(r^2 - R_{i,2}^2)}{(1 - \kappa_2^2)} \right] \quad \text{Eq. 4.2.17}$$

$$v_{z,1} = -\frac{\Delta P_1 R_o^2}{\Delta L_1 4\mu} \left((1 - \kappa_1^2) \left[\frac{\ln\left(\frac{r}{R_o}\right)}{\ln(\kappa_1)} \right] - \left(1 - \frac{r^2}{R_o^2}\right) \right) \quad \text{Eq. 4.2.24}$$

$$v_{z,2} = -\frac{\Delta P_2 R_o^2}{\Delta L_2 4\mu} \left((1 - \kappa_2^2) \left[\frac{\ln\left(\frac{r}{R_o}\right)}{\ln(\kappa_2)} \right] - \left(1 - \frac{r^2}{R_o^2}\right) \right) \quad \text{Eq. 4.2.25}$$

In preparation for Chapter 5, we now define the following dimensionless variables. Refer to Appendix A for a description of the dimensionless group β .

$$\gamma = \frac{r}{R_o} \quad \text{for } R_i < r < R_o \quad \text{Eq. 4.2.26}$$

$$U_{i,j}(\gamma) = \frac{v_{i,j}}{v_s} \quad \text{for } i = \theta, z \text{ and } j = 1, 2 \quad \text{Eq. 4.2.27}$$

$$\beta_{k,j} = \frac{\frac{\Delta P_j R_o^2}{\Delta L_j 4\mu}}{v_s} \quad \text{for } j = 1, 2 \text{ and where } v_s = \Omega_o r \quad \text{Eq. 4.2.28}$$

The variable $\beta_{k,j}$ is the dimensionless ratio of drag and pressure flows, defined in Appendix A, adjusted to fit the cylindrical coordinate system. Applying these scale variables to Eqs. 4.2.15, 4.2.17, 4.2.24, and 4.2.25 gives

$$U_{\theta,1}(\gamma) = \frac{1}{\gamma} \left[\frac{(\gamma^2 - \kappa_1^2)}{(1 - \kappa_1^2)} \right] \quad \text{Eq. 4.2.29}$$

$$U_{\theta,2}(\gamma) = \frac{2}{\gamma} \left[\frac{(\gamma^2 - \kappa_2^2)}{(1 - \kappa_2^2)} \right] \quad \text{Eq. 4.2.30}$$

$$U_{\zeta,1}(\gamma) = -\beta_{\kappa,1} \left((1 - \kappa_1^2) \left[\frac{\ln(\gamma)}{\ln(\kappa_1)} \right] - (1 - \gamma^2) \right) \quad \text{Eq. 4.2.31}$$

$$U_{\zeta,2}(\gamma) = -\beta_{\kappa,2} \left((1 - \kappa_2^2) \left[\frac{\ln(\gamma)}{\ln(\kappa_2)} \right] - (1 - \gamma^2) \right) \quad \text{Eq. 4.2.32}$$

Eqs. 4.2.29 – 4.2.32 thus describe the dimensionless flow of material through the two zones of a kneading element.

The velocity profiles produced in Sections 4.1 and 4.2 are used to describe the flow of material within conveying and kneading elements, respectively. These profiles are used in Chapter 5 to develop explicit solutions for temperature profiles in the extruder. It is shown in the next chapter that these profiles are Sturm-Liouville weight functions; thus, they are required to follow the constraints given by Sturm-Liouville theory. The most significant constraint is that there can be no negative portion to the weight functions. This corresponds to no negative velocity, or no backflow within a screw element. If they are negative, then the temperature profiles produced through the methodology applied in Chapter 5 are not guaranteed to be correct. This thesis considers velocity profiles that show no backflow, in order to ensure the temperature profiles are “protected” by Sturm-Liouville theory.

5. Development of Temperature Profiles

This chapter focuses on the development of temperature profiles within the extruder. As in Chapter 4, the balances of momentum, heat, and mass transfer are applied to individual screw types in order to develop approximations of temperature. The velocity profiles developed in Chapter 4 are important in describing the convective transport of temperature, and are incorporated into the development described in this chapter. Explicit balances are simplified through the use of scaling arguments and the application of dimensionless groups.

5.1 Conveying Elements

The temperature of a polymer processed by SSSP varies greatly with its position in the extruder, and is also dictated by material properties and experimental parameters. Typically, high temperatures are observed in kneading zones. Pressure builds up at these zones, and crushing and shearing of the polymer dissipates large amounts of energy in the form of heat. Conversely, conveying zones have lower temperatures, because no pulverization occurs and yet the polymer is still cooled. As polymer moves through the extruder it passes through multiple kneading and conveying zones, being repeatedly heated and cooled. The polymer eventually develops a steady state temperature profile within the extruder.

Generally, temperature of the material can vary in each of these directions as well as time, and is expressed as

$$T = T(x, y, z, t) \quad \text{Eq. 5.1.1}$$

Each individual screw element contributes a certain change in temperature that can be modeled using a method similar to the one employed in modeling the velocity profile.

The equation of energy is used to develop temperature profiles for a given system in the same way the equation of momentum is used to develop velocity profiles.

In Section 4.1, conveying elements are modeled using a “tilted” coordinate system, marked with prime symbols. The development of temperature profiles for conveying elements follows this same coordinate system. The x' -direction is the screw channel height, the y' -direction is the cross-wise channel direction, and the z' -direction is parallel to the unwound helical channel. Figure 4.1.2 still holds and can be used as a reference for screw geometry. The equation of energy for an incompressible Newtonian fluid with constant thermal conductivity is given as Eq. 5.1.2.

$$\rho \hat{C}_p \left(\frac{\partial T}{\partial t} + v_{x'} \frac{\partial T}{\partial x'} + v_{y'} \frac{\partial T}{\partial y'} + v_{z'} \frac{\partial T}{\partial z'} \right) = k \left[\frac{\partial^2 T}{\partial x'^2} + \frac{\partial^2 T}{\partial y'^2} + \frac{\partial^2 T}{\partial z'^2} \right] + \eta \Phi_v \quad \text{Eq. 5.1.2}$$

In the above equation, ρ is density, \hat{C}_p is heat capacity, T is temperature, t is time, v_i is a given component of the velocity vector, k is thermal conductivity, η is the viscosity, and Φ_v is the dissipation function for a Newtonian fluid. The dissipation function is the source of energy due to internal friction in the polymer flow.

Eq. 5.1.2 represents a balance of convective, conductive, and generational terms that will provide the temperature profile. The term on the left hand side characterizes the convection of heat down the extruder due to the flow of material. The first term on the right hand side represents the conduction of heat from the screw to the barrel (x' -direction), conduction across the element channel (y' -direction), and conduction of heat

down the channel (z' -direction). The last term quantifies any heat generation by viscous dissipation. If heat is generated by another mechanism, such as a chemical reaction, it can be added on to the equation.

At this point, it is unknown as to what mechanism(s) causes heat to be generated within SSSP, and so all potential generation terms are represented by the variable S , where S can be either a constant or a function of position. Eq. 5.1.2 becomes

$$\rho \hat{C}_p \left(\frac{\partial T}{\partial t} + v_x \frac{\partial T}{\partial x'} + v_{y'} \frac{\partial T}{\partial y'} + v_{z'} \frac{\partial T}{\partial z'} \right) = k \left[\frac{\partial^2 T}{\partial x'^2} + \frac{\partial^2 T}{\partial y'^2} + \frac{\partial^2 T}{\partial z'^2} \right] + S \quad \text{Eq. 5.1.3}$$

In Section 4.1, the velocity vector was determined to be only in the z -direction.

$$\vec{v} = v_{z'}(x) \vec{e}_{z'} \quad \text{Eq. 5.1.4}$$

In addition, at steady state operation, time-dependence is dropped. Thus, Eq. 5.1.3 reduces to

$$\rho \hat{C}_p v_{z'} \frac{\partial T}{\partial z'} = k \left[\frac{\partial^2 T}{\partial x'^2} + \frac{\partial^2 T}{\partial y'^2} + \frac{\partial^2 T}{\partial z'^2} \right] + S \quad \text{Eq. 5.1.5}$$

Recall that the y -direction represents the width of the screw channel. It is reasonable to assume that there is little to no variation of temperature in y' , as the order analysis presented in Section 4.1 still holds here. Eq. 5.1.1 becomes

$$T = T(x', z') \quad \text{Eq. 5.1.6}$$

Combining Eqs. 5.1.5 and 5.1.6 results in

$$\rho \hat{C}_p v_{z'} \frac{\partial T}{\partial z'} = k \left[\frac{\partial^2 T}{\partial x'^2} + \frac{\partial^2 T}{\partial z'^2} \right] + S \quad \text{Eq. 5.1.7}$$

Convection and conduction both operate in the z' -direction. These two mechanisms of heat transfer are acting in parallel, transporting heat down the length of

the extruder. The Péclet number is a dimensionless group that compares these two processes.

$$Pe = \frac{Lv}{\alpha} = \frac{\text{convective rate in } z'}{\text{conductive rate in } z'} \quad \text{Eq. 5.1.8}$$

L is the characteristic length, v is the velocity, and α is the thermal diffusivity. Large values of Pe indicate that convective processes dominate over conductive processes.

Smaller values of Pe indicate that conductive processes dominate. The thermal diffusivities of polymers are typically quite small, and so Péclet numbers for polymeric systems are generally large [37]. The molecular process of axial conduction is therefore assumed to be insignificant when compared to the macroscopic process of convection. As a result, Eq. 5.1.7 becomes

$$\rho \hat{C}_p v_{z'} \frac{\partial T}{\partial z'} = k \frac{\partial^2 T}{\partial x'^2} + S \quad \text{Eq. 5.1.9}$$

Eq. 5.1.9 states that the convection of heat in the z' -direction is balanced by the conduction of heat in the x -direction and the generation of heat throughout the material.

The following variables are defined to non-dimensionalize Eq. 5.1.9.

$$\xi' = \frac{x'}{H} \quad \text{Eq. 5.1.10a}$$

$$\zeta' = \frac{z'}{L} \quad \text{Eq. 5.1.10b}$$

$$\theta = \frac{[T - T_b]}{[T_s - T_b]} \quad \text{Eq. 5.1.10c}$$

$$\psi = \frac{S}{S_c} \quad \text{Eq. 5.1.10d}$$

Applying Eqs. 5.1.10a – 5.1.10d to Eq. 5.1.9 gives

$$\rho \hat{C}_p v_{z'} \frac{[T_s - T_b]}{L} \frac{\partial \theta}{\partial \zeta'} = k \frac{[T_s - T_b]}{H^2} \frac{\partial^2 \theta}{\partial \xi'^2} + \psi S_c \quad \text{Eq. 5.1.11}$$

With rearrangement, we have

$$\frac{\rho \hat{C}_p v_{z'}(x') H^2}{kL} \frac{\partial \theta}{\partial \zeta'} = \frac{\partial^2 \theta}{\partial \xi'^2} + \frac{S_c H^2}{k[T_s - T_b]} \psi \quad \text{Eq. 5.1.12}$$

In the above equation, $v_{z'}$ is a function of x' (ξ' , as well). Therefore, $v_{z'}$ must also be non-dimensionalized, and has the following dimensionless form.

$$U(\xi') = \frac{v_{z'}(x')}{v_s} \quad \text{Eq. 5.1.13}$$

Where v_s is a scale velocity, and with rearrangement $v_{z'}$ becomes

$$v_{z'} = v_s U(\xi') \quad \text{Eq. 5.1.14}$$

The dimensionless function $U(\xi')$ characterizes the general shape of the velocity profile within conveying elements, and is derived in section 4.1 (Eq. 4.1.45).

Inserting Eq. 5.1.14 into Eq. 5.1.12 leads to

$$\frac{\rho \hat{C}_p v_s U(\xi') H^2}{kL} \frac{\partial \theta}{\partial \zeta'} = \frac{\partial^2 \theta}{\partial \xi'^2} + \frac{S_c H^2}{k[T_s - T_b]} \psi \quad \text{Eq. 5.1.15}$$

The final term can be bundled into one variable, Ω , for the sake of book keeping.

A discussion on Ω is included in Appendix B. H , k , T_s , and T_b are all constants; ψ is unspecified at this point, and as discussed earlier for the variable S , can be either a constant, a function of ξ' , a function of ζ' , or a function of both. At this point, we will consider constant generation such that S is independent of position. With some rearrangement, Eq. 5.1.15 then becomes

$$\frac{\rho \hat{C}_p v_s H^2}{kL} U(\xi') \frac{\partial \theta}{\partial \zeta'} = \frac{\partial^2 \theta}{\partial \xi'^2} + \Omega \quad \text{Eq. 5.1.16}$$

The coefficient of the first term can be expressed in terms of the Graetz number, denoted by Gz

$$Gz = \frac{H}{L} Re Pr = \frac{\text{convection in } z'}{\text{conduction in } x'} \quad \text{Eq. 5.1.17}$$

This number characterizes the thermal development of a given flow system and is a function of the Reynolds and Prandtl numbers. Smaller Graetz numbers indicate higher thermal development for a system, and large values indicate no thermal development.

The Reynolds number, Re , characterizes the flow-type of a system as laminar, transitional, and turbulent flow, and is the ratio of inertial to viscous forces.

$$Re = \frac{\rho H v}{\mu} = \frac{\text{inertial forces}}{\text{viscous forces}} \quad \text{Eq. 5.1.18}$$

The Prandtl number, Pr , characterizes a given system and its ability to diffuse momentum versus its ability to diffuse heat.

$$Pr = \frac{\hat{c}_p \mu}{k} = \frac{\text{viscous diffusion}}{\text{thermal diffusion}} \quad \text{Eq. 5.1.19}$$

Inserting Eqs. 5.1.18 and 5.1.19 into Eq. 5.1.17 gives the following expression for Gz .

$$Gz = \frac{\rho \hat{c}_p v_s H^2}{kL} = \frac{\text{convection in } z'}{\text{conduction in } x'} \quad \text{Eq. 5.1.20}$$

As can be seen, Eq. 5.1.20 is exactly the coefficient found preceding the first term in Eq. 5.1.16. The equation can be written in the following form.

$$Gz U(\xi') \frac{\partial \theta}{\partial \zeta'} = \frac{\partial^2 \theta}{\partial \xi'^2} + \Omega \quad \text{Eq. 5.1.21}$$

Incidentally, the Péclet number used earlier is also defined as the product of the Reynolds and Prandtl numbers. Pe describes convection and conduction in *parallel*, whereas Gz describes *perpendicular* convection and conduction. The $\frac{H}{L}$ coefficient is responsible for translating the parallel Pe to the perpendicular Gz . Figure 5.1.1 compares the Péclet and Graetz scenarios relevant to this study.

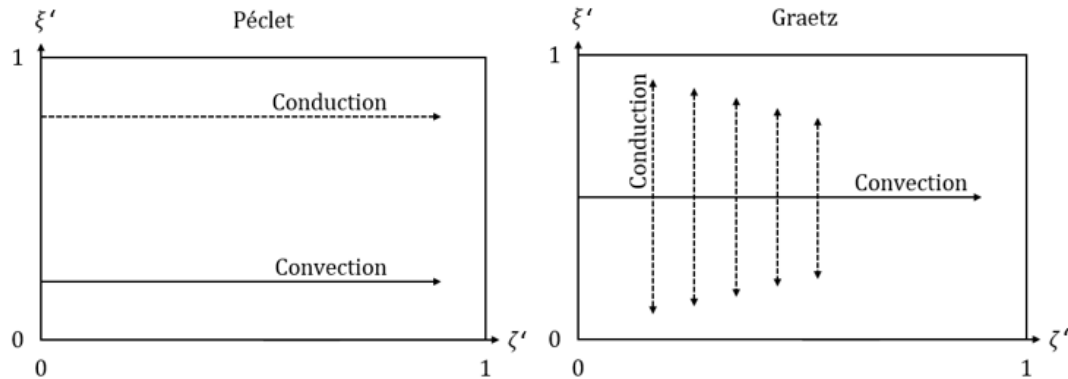


Figure 5.1.1: Péclet versus Graetz flow types; Péclet considers heat transfer competing in parallel, Graetz considers perpendicularly competing heat transfer

Both the Péclet number and Graetz number are important for this study, as they give insight to the characteristics of flow within the extruder.

Graetz numbers are functions of material and flow properties as shown by Eq. 5.1.20. A flow can be considered thermally developed when the Graetz number is approximately 1000 or less (see Eq. 5.1.35; when the Gz is greater than ~ 1000 , the exponential given in Eq. 5.1.35 does not decay quickly enough to give a thermally developed flow.) In these thermally developed situations, it is more reasonable to apply a separation of variables method to solve Eq. 5.1.21 [28]. Separation of variables does well at characterizing the solution farther away from the initial conditions. When the Graetz number is greater than 1000, the flow cannot be considered thermally developed, and therefore the method of combination of variables is more useful for solving Eq. 5.1.21. Combination of variables does well at characterizing the initial development of a flow, and is less precise farther from the initial conditions [38]. The Gz in SSSP is predicted to be below 1000 for SSSP elements; for example, polypropylene moving through a

conveying element has a Gz of approximately 100 [calculated using Eq. 5.1.20]. As a result, separation of variables is appropriate to apply to solve Eq. 5.1.21.

Eq. 5.1.21 requires three boundary conditions in order to be solved. Two of these are in x' , and one of these is in z' . The dimensional boundary conditions on the system are as follows.

$$T(x' = 0, z') = T_s \quad \text{Eq. 5.1.22a}$$

$$T(x' = H, z') = T_b \quad \text{Eq. 5.1.22b}$$

$$T(x', z' = 0) = T_o \quad \text{Eq. 5.1.22c}$$

In dimensionless form, the boundary conditions are:

$$\theta(\xi' = 0, \zeta') = 1 \quad \text{Eq. 5.1.23a}$$

$$\theta(\xi' = 1, \zeta') = 0 \quad \text{Eq. 5.1.23b}$$

$$\theta(\xi', \zeta' = 0) = \theta_o \quad \text{Eq. 5.1.23c}$$

Eq. 5.1.21 is an inhomogeneous partial differential equation due to the source term Ω , with boundary conditions that are also inhomogeneous. Direct application of separation of variables will not work in such a setting, and so the PDE must be further manipulated. The principle of superposition is applied here, where the complete solution for dimensionless temperature is decomposed into two individual solutions. The dimensionless temperature, θ , can be broken into two separate parts; one is dependent on both ξ' and ζ' , where the other is only dependent on ξ' and is independent of ζ' . That is,

$$\theta(\xi', \zeta') = \theta_1(\xi') + \theta_2(\xi', \zeta') \quad \text{Eq. 5.1.24}$$

The two distinct differential equation problems, derived by applying Eq. 5.1.24 to Eq. 5.1.21 and Eqs. 5.1.23a – 5.1.23c, are shown in Table 5.1.1.

Table 5.1.1: Decomposition to ODE and PDE problems

Full PDE $\theta(\xi', \zeta')$	Problem 1 $\theta_1(\xi')$	Problem 2 $\theta_2(\xi', \zeta')$
$Gz U(\xi') \frac{\partial \theta}{\partial \zeta'} = \frac{\partial^2 \theta}{\partial \xi'^2} + \Omega$ 5.1.21	$0 = \frac{d^2 \theta_1}{d \xi'^2} + \Omega$ 5.1.25	$Gz U(\xi') \frac{\partial \theta_2}{\partial \zeta'} = \frac{\partial^2 \theta_2}{\partial \xi'^2}$ 5.1.26
$\theta(\xi' = 0, \zeta') = 1$ 5.1.23a	$\theta_1(\xi' = 0) = 1$ 5.1.27a	$\theta_2(\xi' = 0, \zeta') = 0$ 5.1.28a
$\theta(\xi' = 1, \zeta') = 0$ 5.1.23b	$\theta_1(\xi' = 1) = 0$ 5.1.27b	$\theta_2(\xi' = 1, \zeta') = 0$ 5.1.28b
$\theta(\xi', \zeta' = 0) = \theta_o$ 5.1.23c	--	$\theta_2(\xi', \zeta' = 0) = \theta_o - \theta_1(\xi')$ 5.1.28c

Problem 1 is solved by integrating Eq. 5.1.25 twice with respect to ξ' and then applying the boundary conditions in Eqs. 5.1.27a and 5.1.27b. The result is

$$\theta_1(\xi') = (1 - \xi') \left(1 + \frac{\Omega}{2} \xi' \right) \quad \text{Eq. 5.1.29}$$

Problem 2 focuses on a partial differential equation that can be solved using a separation of variables approach. Proposing the separated solution as

$$\theta_2(\xi', \zeta') = X(\xi')Y(\zeta') \quad \text{Eq. 5.1.30}$$

converts Eq. 5.1.26 to

$$Gz U(\xi')X(\xi') \frac{dY(\zeta')}{d\zeta'} = \frac{d^2 X(\xi')}{d\xi'^2} Y(\zeta') \quad \text{Eq. 5.1.31}$$

Rearranging Eq. 5.1.31 gives two distinct, yet connected, ordinary differential equations for $X(\xi')$ and $Y(\zeta')$

$$\frac{d^2 X(\xi')}{d\xi'^2} \frac{1}{U(\xi')X(\xi')} = Gz \frac{1}{Y(\zeta')} \frac{dY(\zeta')}{d\zeta'} = \mu \quad \text{Eq. 5.1.32}$$

Although the result is completely separated, the two sides of Eq. 5.1.32 are still equal to one another. Consequently, they are both then equal to some constant value, written as μ .

The functions $X(\xi')$ and $Y(\zeta')$ are now broken into the two distinct ODE's.

$$\frac{d^2 X(\xi')}{d\xi'^2} - \mu U(\xi')X(\xi') = 0 \quad \text{Eq. 5.1.33}$$

$$Gz \frac{dY(\zeta')}{d\zeta'} - \mu Y(\zeta') = 0 \quad \text{Eq. 5.1.34}$$

Eq. 5.1.34 has the following general solution

$$Y(\zeta') = Ae^{\mu\zeta'/Gz} \quad \text{Eq. 5.1.35}$$

Where A is a constant of integration.

Eq. 5.1.33 can be solved for positive, zero, or negative values of μ . In this particular case, μ is set equal to the value $-\lambda^2$. This is done because the dependence of the complete dimensionless temperature profile is expected to evolve into a function of *only* ξ' at large values of ζ' (i.e. the system becomes thermally developed and $\left. \frac{\partial \theta}{\partial \zeta'} \right|_{\zeta' \rightarrow \infty} \rightarrow$

0). Revisiting Eq. 5.1.24 shows that all dependence on ζ' is contained to θ_2 , and thus $\theta_2(\xi', \zeta') \rightarrow 0$ as $\zeta' \rightarrow \infty$. This gives

$$\frac{d^2 X(\xi')}{d\xi'^2} + \lambda^2 U(\xi')X(\xi') = 0 \quad \text{Eq. 5.1.36}$$

The boundaries on this particular situation are homogeneous, as follows.

$$X(\xi' = 0) = 0 \quad \text{Eq. 5.1.37a}$$

$$X(\xi' = 1) = 0 \quad \text{Eq. 5.1.37b}$$

Eq. 5.1.36 is a Sturm-Liouville eigenvalue problem. Eqs. 5.1.37a and 5.1.37b were derived by applying Eq. 5.1.30 to Eqs. 5.1.28a and 5.1.28b.

Solutions to Sturm-Liouville eigenvalue problems have an infinite set of solutions, defined by a series of corresponding eigenvalues and eigenfunctions. Eq. 5.1.38 shows the structure of the complete solution to Eq. 5.1.36

$$X(\xi') = \sum_{n=1}^{\infty} A_n F_n(\lambda_n; \xi') \quad \text{Eq. 5.1.38}$$

Where λ_n is an eigenvalue, $F_n(\lambda_n; \xi')$ is the corresponding eigenfunction, and A_n is a constant. The eigenfunctions generated by Sturm-Liouville equations are defined to be orthogonal, which allows A_n to be calculated by

$$A_n = \frac{\langle \theta_0 - \theta_1(\xi'), F_n \rangle}{\langle F_n, F_n \rangle} \quad \text{Eq. 5.1.39}$$

The term $\theta_0 - \theta_1(\xi')$ is generated by the boundary condition given above as Eq. 5.1.28c.

The inner products in Eq. 5.1.39 are defined by

$$\langle F_n, F_m \rangle = \int_0^1 F_n(\lambda_n; \xi') F_m(\lambda_m; \xi') U(\xi') d\xi' \quad \text{Eq. 5.1.40}$$

where inner product measures the projection of one function onto another. F_n are orthogonal (i.e. linearly independent) such that the calculation in Eq. 5.1.40 is equal to zero for $n \neq m$. The function $U(\xi')$ is the dimensionless velocity profile, which is written as

$$U(\xi') = \frac{2\xi'}{(1+\varphi)} \quad \text{Eq. 4.1.42}$$

In Eq. 5.1.36, by Sturm-Liouville theory, $U(\xi')$ is a weight function which must always be positive. If the weight function is not always positive, then the orthogonality of

the resulting eigenfunctions is not guaranteed, rendering this solution methodology ineffective. Generally speaking, this limit translates into a prohibition of backflow in the extruder; that is, no material can have a negative velocity ($U(\xi')$ is always positive). For the case of conveying elements, it is known that material *never* flows backwards in the helical channel; after passing a particular point in space, a particle will not return to that point [17]. In terms of the variable β from Appendix A, $\beta = 1$ is the upper limit on values of β for conveying elements. For this case the weight function $U(\xi')$ is thus always positive and orthogonality of the eigenfunction solutions to Eq. 5.1.36 is guaranteed. The case with $\beta = 0$ corresponds to pure drag flow with no effects of pressure on the system, and the weight function remains positive. Negative values of β are possible, but unlikely in conveying elements, as this indicates a forward pushing pressure (conveying elements exhibit *competing* forward drag and reverse back pressure flows). Therefore, β can be limited to the range of 0 to 1 for conveying elements, although in the case of SSSP most scenarios will reflect $\beta = 0$. This discussion will concern pure drag flow, where $\beta = 0$. The case of $\beta = 1$ and its effects on velocity and temperature are discussed in Appendix A. Using the value of $\beta = 0$ for $U(\xi')$ in Eq. 5.1.36 gives

$$\frac{d^2 X(\xi')}{d\xi'^2} + \lambda^2 \xi' X(\xi') = 0 \quad \text{for } \beta = 0 \quad \text{Eq. 5.1.43}$$

Eq. 5.1.43 is of the form

$$y''(x) + kx^m y(x) = 0 \quad \text{Eq. 5.1.44}$$

where $k = \lambda^2$, y is X , x is ξ' , and m is either 1 or 2. The solution to Eq. 5.1.43 can be represented by Bessel functions [39]. Differential equations of the form of Eq. 5.1.44 have the following general solution

$$y(x) = c_1 \sqrt{\xi} J_{\frac{1}{m+2}} \left(\frac{2\sqrt{k}}{m+2} x^{\frac{m+2}{2}} \right) + c_2 \sqrt{\xi} J_{-\frac{1}{m+2}} \left(\frac{2\sqrt{k}}{m+2} x^{\frac{m+2}{2}} \right) \text{ where } mk \neq -2k$$

Eq. 5.1.45

The solution is expressed in terms of Bessel functions, J_p , of order p , where

$$p = \frac{1}{m+2}$$

Eq. 5.1.46

Applying Eq. 5.1.46 to Eq. 5.1.45 gives the general solution for the case of $\beta = 0$ as

$$X(\xi') = c_1 \sqrt{\xi'} J_{\frac{1}{3}} \left(\frac{2}{3} \lambda \xi'^{\frac{3}{2}} \right) + c_2 \sqrt{\xi'} J_{-\frac{1}{3}} \left(\frac{2}{3} \lambda \xi'^{\frac{3}{2}} \right)$$

Eq. 5.1.47

At $\xi' = 0$, Bessel functions of positive order are equal to 0 and Bessel functions of negative order are 1. The boundary condition thus leads to

$$X(\xi') = c_1 \sqrt{\xi'} J_{\frac{1}{3}} \left(\frac{2}{3} \lambda \xi'^{\frac{3}{2}} \right)$$

Eq. 5.1.48

Eq. 5.1.48 states the eigenfunction relation for the case of $\beta = 0$ as roots of $J_{\frac{1}{3}}$. Applying the second boundary condition, Eq. 5.1.28b, gives the following relationship

$$0 = c_1 J_{\frac{1}{3}} \left(\frac{2}{3} \lambda_n \right)$$

Eq. 5.1.49

Non-trivial solutions exist for values of λ_n which correspond to the zero roots of the appropriate order Bessel function. Bessel functions naturally oscillate about zero, and thus pass through an infinite amount of roots as the function increases. Each of these roots contribute an eigenvalue that then provides an eigenfunction. The resulting infinite set of eigenfunctions fulfills the series solution proposed in Eq. 5.1.38. Revisiting Eq.

5.1.30 shows that the eigenfunction series (i.e. $X(\xi')$) is balanced by a decaying exponential (i.e. $Y(\zeta')$, or, Eq. 5.1.35), and the product of these two functions is the solution for $\theta_2(\xi', \zeta')$. The solution for $\theta_2(\xi', \zeta')$ for the specific case of $\beta = 0$ is thus

$$\theta_2(\xi', \zeta') = \sum_{n=1}^{\infty} A_n \exp\left(\frac{-\lambda_n^2 \zeta'}{Gz}\right) \sqrt{\xi'} J_{\frac{1}{3}}\left(\frac{2}{3} \lambda_n \xi'^{\frac{3}{2}}\right) \quad \text{Eq. 5.1.50}$$

Applying Eqs. 5.1.24 and 5.1.29 to Eq. 5.1.50 gives

$$\theta(\xi', \zeta') = (1 - \xi') \left(1 + \frac{\Omega}{2} \xi'\right) + \sum_{n=1}^{\infty} A_n \exp\left(\frac{-\lambda_n^2 \zeta'}{Gz}\right) \sqrt{\xi'} J_{\frac{1}{3}}\left(\frac{2}{3} \lambda_n \xi'^{\frac{3}{2}}\right) \quad \text{Eq. 5.1.51}$$

Eq. 5.1.51 gives the analytical solution for the dimensionless temperature profile in the channel of a conveying element, for the specific case of $\beta = 0$.

This analytical solution and the solution for the case of $\beta = 1$ are the lower and upper bounds on the behavior of flow within a conveying element, respectively. In many applications, the first eigenvalue and first eigenfunction are sufficient in approximating a system's general behavior, as the exponential rapidly devolves to unity. As the flow develops in the ζ' -direction, the exponential term collapses to zero and the system only varies in ξ' . In this particular case, the Graetz number controls the rate of decay of the exponential. As Graetz numbers decrease in value (i.e. transverse conduction outweighs axial convection) the exponential decays faster and the profile approaches $\theta_1(\xi')$ more rapidly. The expected Graetz numbers for this scenario are expected to be no higher than ~ 250 . At this value, the exponential does not appreciably vanish through ζ' until the eighth eigenvalue and eigenfunction pair.

The first eight eigenvalues and the corresponding constants A_n are given in Table 5.1.2 for the case of $\beta = 0$. The constants A_n are evaluated using Eq. 5.1.39.

Table 5.1.2: First eight eigenvalues and corresponding constants

$\beta = 0$		
n	λ_n	A_n
1	4.35388...	0.3535...
2	9.04912...	-1.2785...
3	13.75576...	0.3747...
4	18.46529...	-1.0910...
5	23.17597...	0.3737...
6	27.88723...	-0.9965...
7	32.59881...	0.3703...
8	37.31060...	-0.9353...

The first eight eigenfunctions for $\beta = 0$ are then given in Figure 5.1.2.

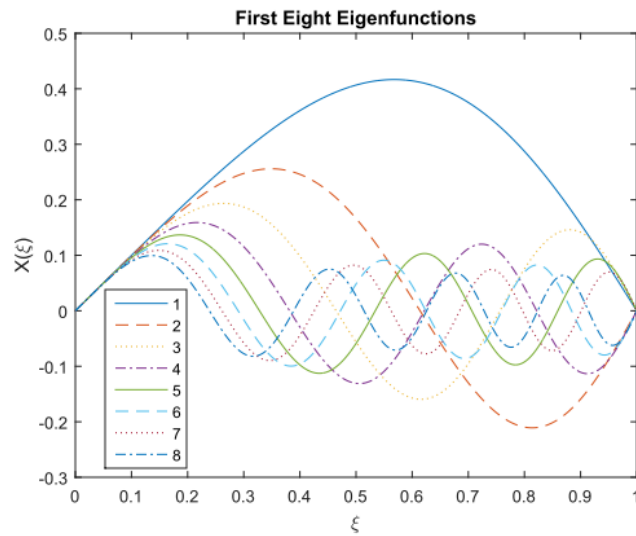


Figure 5.1.2: First eight eigenfunctions that contribute to the series solution for $X(\xi')$ for $\beta = 0$

The eigenfunctions shown in Figure 5.1.2 are the first eight of an infinite set of functions. As the number of the term increases the overall summation approaches the full solution. The first eigenfunction gives an approximation of the variation of $X(\xi')$ with ξ' . The inclusion of higher order eigenfunctions modifies the profile, and the sum of the infinite set eigenfunctions yields the exact variation of $X(\xi')$ with ξ' . The sum of each of the first eight eigenfunctions is shown in Figures 5.1.3.

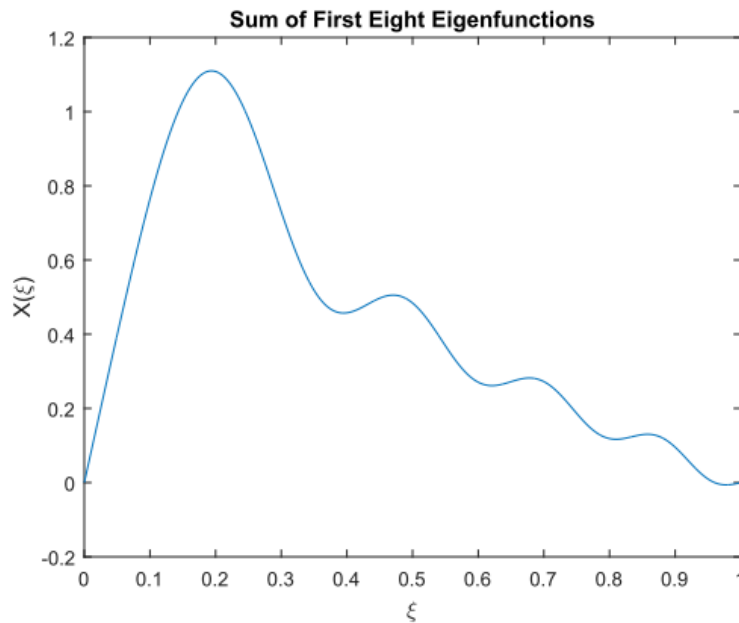


Figure 5.1.3: $[\sum_{n=1}^8 A_n F_n(\lambda_n; \xi')]$ Sum of the first eight eigenfunctions that contribute to the solution for $X(\xi')$ for $\beta = 0$

Figure 5.1.3 shows an oscillatory profile that does not fully represent $X(\xi')$ for $\beta = 0$ (or $\beta = 1$, as discussed in Appendix A). These oscillations are a result of overlaying a small number of eigenfunctions, and will appear to distort the resulting solution until $n \rightarrow \infty$; however, the utility of these first eight eigenfunctions lies in their averages through ξ' . The averages are useful because they capture the general magnitude

of each eigenfunction, but help dampen any oscillations that appear due to the small number of overlaid terms. Eq. 5.1.51 shows that the eigenfunctions only vary in the ξ' -direction, while flow is in the ζ' -direction.

The evolution of temperature in the ζ' -direction can be approximated through taking the average of Eq. 5.1.51 through ξ' , resulting in a function that only varies in ζ' .

The resulting average through the first eight eigenfunctions is written as

$$\bar{\theta}(\zeta') = \left(\frac{1}{2} + \frac{\Omega}{12}\right) + \sum_{n=1}^8 A_n \exp\left(\frac{-\lambda_n^2 \zeta'}{Gz}\right) \bar{F}_n(\lambda_n) \quad \text{Eq. 5.1.52}$$

The first eight terms are expected to adequately approximate the full solution. By Sturm-Liouville theory, the complete solution to the differential equation is a converging infinite series of functions. It is assumed that partial sums of this series do converge as well; however, future work can focus determining the validity of this assumption.

The averaged eigenfunctions $\bar{F}_n(\lambda_n)$ are constant values that are paired with their respective eigenvalues. They are given in Table 5.1.3.

Table 5.1.3: Average values of the first eight eigenfunctions for conveying element flow

$\beta = 0$	
n	$\bar{F}_n(\lambda_n)$
1	0.26075...
2	0.04655...
3	0.04928...
4	0.02042...
5	0.02343...
6	0.01242...
7	0.01448...
8	0.00868...

The values of the averaged eigenfunctions in Table 5.1.3 can be used with Eq. 5.1.52 to produce profiles of dimensionless temperature as a function of ζ' . Figure 5.1.4 shows how increasing the number of terms in the series solution increases the accuracy of the predicted profile.

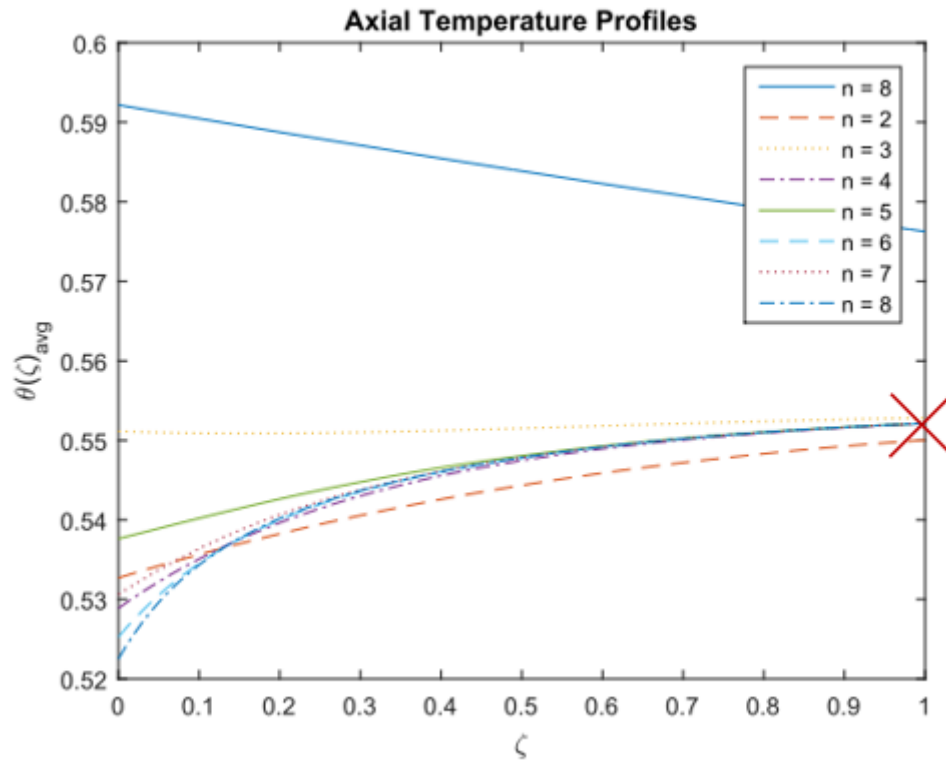


Figure 5.1.4: Comparison of the effectiveness of various series solutions for $\beta = 0$

As the value of n increases (i.e. more terms are included in the eigenfunction series), the average dimensionless temperature approaches a relatively consistent final value.

Although the profiles vary initially, they all converge to approximately the same value when $n > 4$, marked with an “X” in Figure 5.1.4. This final value is the exit temperature of material when it leaves a single screw element, and therefore is the initial condition,

θ_o , for the next element in the screw. The solutions converge to a consistent value, indicating that the “new” θ_o can be confidently calculated with a relatively small number of terms.

The averaged solution proposed in Eq. 5.1.54 can be applied to the cases of $\beta = 0$, $\beta = 1$, and any value of β between the two. A numerical solution can be applied to the same effect for the values of β that do not yield analytical solutions (i.e. any value that is between 0 and 1). The analytical result proposed in this section and the result discussed in Appendix A serve as a basis for any numerical calculations.

5.2 Kneading Elements

In Section 4.2, the flow profiles of kneading elements are developed on the basis of a cylindrical coordinate system. In order to develop temperature profiles for kneading elements, a cylindrical coordinate system is once again applied. We begin, as in Section 5.1, with the equation of energy. The equation of energy in cylindrical coordinates is written as

$$\rho \hat{C}_p \left(\frac{\partial T}{\partial t} + v_r \frac{\partial T}{\partial r} + \frac{v_\theta}{r} \frac{\partial T}{\partial \theta} + v_z \frac{\partial T}{\partial z} \right) = k \left[\frac{1}{r} \frac{\partial}{\partial r} \left(r \frac{\partial T}{\partial r} \right) + \frac{1}{r^2} \frac{\partial^2 T}{\partial \theta^2} + \frac{\partial^2 T}{\partial z^2} \right] + \eta \Phi_v$$

Eq. 5.2.1

The kneading elements are thought to rotate such that they can be approximated by concentric cylinders, as described in Section 4.2. The magnitude of velocity in the θ -direction is much larger than that in the z -direction, such that no gradients of temperature

can develop through θ . Therefore, all dependence of temperature on θ can be ignored.

We also assign the heat generation to a more general term, S . This reduces Eq. 5.2.1 to

$$\rho \hat{C}_p \left(\frac{\partial T}{\partial t} + v_r \frac{\partial T}{\partial r} + v_z \frac{\partial T}{\partial z} \right) = k \left[\frac{1}{r} \frac{\partial}{\partial r} \left(r \frac{\partial T}{\partial r} \right) + \frac{\partial^2 T}{\partial z^2} \right] + S \quad \text{Eq. 5.2.2}$$

Section 4.2 develops the governing velocity profiles for kneading elements. In that section, the velocity field is found to have components only in the θ - and z -directions, such that there is no r -component to the velocity. While also considering steady state, Eq. 5.2.2 becomes

$$\rho \hat{C}_p v_z \frac{\partial T}{\partial z} = k \left[\frac{1}{r} \frac{\partial}{\partial r} \left(r \frac{\partial T}{\partial r} \right) + \frac{\partial^2 T}{\partial z^2} \right] + S \quad \text{Eq. 5.2.3}$$

This equation is similar to Eq. 5.1.7, where conduction operates both in parallel with and perpendicular to the convective flow of heat. The same Pe argument can be made here, and convection in z can be assumed to greatly outweigh conduction in z . As a result, Eq. 5.2.3 transforms into

$$\rho \hat{C}_p v_z \frac{\partial T}{\partial z} = k \left[\frac{1}{r} \frac{\partial}{\partial r} \left(r \frac{\partial T}{\partial r} \right) \right] + S \quad \text{Eq. 5.2.4}$$

With the exception of the first term on the right hand side, Eq. 5.2.4 is identical to the governing equation for conveying elements.

The boundary conditions on flow in kneading elements are the same as for flow in conveying elements.

$$T(r = R_i, z) = T_s \quad \text{Eq. 5.2.5a}$$

$$T(r = R_o, z) = T_b \quad \text{Eq. 5.2.5b}$$

$$T(r, z = 0) = T_o \quad \text{Eq. 5.2.5c}$$

We continue with this temperature profile development in a similar manner to that of conveying elements. In order to approach analytical results, we apply the principle of superposition and propose

$$T(r, z) = T_1(r) + T_2(r, z) \quad \text{Eq. 5.2.6}$$

The principle of superposition formulates two complete boundary value problems, which are shown in Table 5.2.1.

Table 5.2.1: Decomposition to ODE and PDE problems

Problem 1 $T_1(r)$	Problem 2 $T_2(r, z)$
$0 = k \left[\frac{1}{r} \frac{\partial}{\partial r} \left(r \frac{\partial T_1}{\partial r} \right) \right] + S$ <p style="text-align: center;">5.2.7</p>	$\rho \hat{C}_p v_z \frac{\partial T_2}{\partial z} = k \left[\frac{1}{r} \frac{\partial}{\partial r} \left(r \frac{\partial T_2}{\partial r} \right) \right] \quad 5.2.8$
$T_1(r = R_i) = T_s \quad 5.2.9a$	$T_2(r = R_i, z) = 0 \quad 5.2.10a$
$T_1(r = R_o) = T_b \quad 5.2.9b$	$T_2(r = R_o, z) = 0 \quad 5.2.10b$
--	$T_2(r, z = 0) = T_o - T_1(r) \quad 5.2.10c$

The problems formulated in Table 5.2.1 are similar to those proposed in Table 5.1.1, and the solution methodology follows the same path. We begin by determining the solution to the “steady” profile, $T_1(r)$. Eq. 5.1.7 is of the same form as the differential equation that governs the circumferential velocity profile. It considers S rather than the

pressure drop, k rather than μ , and T_1 rather than v_z . Therefore, the general solution is the same as that proposed in Eq. 4.2.22, with the replacements prescribed above.

$$T_1 = \frac{Sr^2}{4k} + c_1 \ln(r) + c_2 \quad \text{Eq. 5.2.11}$$

Applying the boundary conditions prescribed in Eqs. 5.1.9a and 5.1.9b gives

$$T_1 = T_b + \frac{SR_o^2}{4k} \left[(1 - \kappa^2) \left[\frac{\ln\left(\frac{r}{R_o}\right)}{\ln(\kappa)} \right] - \left(1 - \frac{r^2}{R_o^2}\right) \right] + [T_s - T_b] \left(\frac{\ln\left(\frac{r}{R_o}\right)}{\ln(\kappa)} \right) \quad \text{Eq. 5.2.12}$$

We now define the following scale variables

$$\theta_1 = \frac{T_1 - T_b}{T_s - T_b} \quad \text{Eq. 5.2.13a}$$

$$\gamma = \frac{r}{R_o} \quad \text{for } R_i < r < R_o \quad \text{Eq. 5.2.13b}$$

$$\Omega = \frac{SR_o^2}{4k[T_s - T_b]} \quad \text{Eq. 5.2.13c}$$

$$\zeta = \frac{z}{L} \quad \text{Eq. 5.2.13d}$$

Applying these scale variables to Eq. 5.2.12 gives the dimensionless “steady” temperature profile

$$\theta_1 = \left[\frac{\ln(\gamma)}{\ln(\kappa)} \right] + \Omega \left[(1 - \kappa^2) \left[\frac{\ln(\gamma)}{\ln(\kappa)} \right] - (1 - \gamma^2) \right] \quad \text{Eq. 5.2.14}$$

We now move on to the second problem given in Table 5.2.1, which describes the “unsteady” portion of flow. As with conveying elements, the flow here is a balance of perpendicular conduction and convection, Graetz-type flow. Consequently, we must define a Graetz number for these cylindrical coordinates. The cylindrical Graetz number is

$$Gz = \frac{\rho \hat{c}_p v_s R_o^2}{kL} \quad \text{Eq. 5.2.15}$$

Using the above dimensionless groups we can non-dimensionalize Eq. 5.2.8, giving

$$Gz U_\zeta(\gamma) \frac{\partial \theta_2}{\partial \zeta} = \frac{1}{\gamma} \frac{\partial}{\partial \gamma} \left(\gamma \frac{\partial \theta_2}{\partial \gamma} \right) \quad \text{Eq. 5.2.16}$$

Eq. 5.2.16 is a partial differential equation the radial and axial directions. We can further simplify this differential equation in a similar way to Section 5.1. We assume the solution $\theta_2(\gamma, \zeta)$ is separable as follows

$$\theta_2(\gamma, \zeta) = X(\gamma)Y(\zeta) \quad \text{Eq. 5.2.17}$$

Applying Eq. 5.2.17 to Eq. 5.2.16 gives two separate differential equations in γ and ζ .

They are written as

$$Y'(\zeta) - \mu Gz Y(\zeta) = 0 \quad \text{Eq. 5.2.18}$$

$$\frac{d}{d\gamma} (\gamma X'(\gamma)) - \mu \gamma U_\zeta(\gamma) X(\gamma) = 0 \quad \text{Eq. 5.2.19}$$

The differential equation describing $Y(\zeta)$ is identical to that discussed in Section 5.1. Its general solution is an exponential, and if we assume $\mu = -\lambda^2$ (same logic as in Section 5.1), then it can be written as

$$Y(\zeta) = c_1 \exp\left(\frac{-\lambda^2 \zeta}{Gz}\right) \quad \text{Eq. 5.2.20}$$

The remainder of the solution is treated almost identically to that in Section 5.1. This system is also a Sturm-Liouville eigenvalue problem, and the discussion in Section 5.1 still applies. The axial velocity profiles $U_\zeta(\gamma)$ are again the weight functions, which *cannot* be negative. They are given as Eqs. 4.2.31 and 4.2.32. In the case of kneading elements, flow is expected to be driven forward by pressure gradients, such that these

profiles do satisfy their role as weight functions. Eq. 5.2.19 can be solved using numerical methods in MATLAB.

The solution to Eq. 5.2.16 is developed from the individual solutions of $X(\gamma)$ and $Y(\zeta)$. Where we know the analytical form of $Y(\zeta)$, we assign the solution for $X(\gamma)$ as some function

$$X(\gamma) = \sum_{n=1}^{\infty} A_n F_n(\lambda_n; \gamma) \quad \text{Eq. 5.2.21}$$

The constants A_n are determined via the same calculation as presented in Section 5.1, which is rewritten here as

$$A_n = \frac{\langle \theta_o - \theta_1(\gamma), F_n \rangle}{\langle F_n, F_n \rangle} \quad \text{Eq. 5.2.22}$$

Combining this proposed form of $X(\gamma)$ with the solution for $Y(\zeta)$, we find

$$\theta_2(\gamma, \zeta) = \sum_{n=1}^{\infty} A_n \exp\left(\frac{-\lambda_n^2 \zeta}{Gz}\right) F_n(\lambda_n; \gamma) \quad \text{Eq. 5.2.23}$$

This result is identical to the one found in Section 5.1 for conveying elements. The difference here lies in the numerical calculation of the eigenvalues and eigenfunctions, as they result from a different differential equation. Reapplying the definition of superposition, we find the solution for the dimensionless temperature profile in kneading elements is

$$\theta(\gamma, \zeta) = \left[\frac{\ln(\gamma)}{\ln(\kappa)} \right] + \Omega \left[(1 - \kappa^2) \left[\frac{\ln(\gamma)}{\ln(\kappa)} \right] - (1 - \gamma^2) \right] + \sum_{n=1}^{\infty} A_n \exp\left(\frac{-\lambda_n^2 \zeta}{Gz}\right) F_n(\lambda_n; \gamma) \quad \text{Eq. 5.2.24}$$

The characteristics of this equation are quite similar to Eq. 5.1.51. The first two terms on the right hand side describe the “steady” portion of the temperature profile, the approach to which is characterized by the last term, the “unsteady” portion. The same

averaging concept is applied here, where the profile is “smoothed” in the radial direction.

The resulting averaged profile for temperature in a kneading element is

$$\bar{\theta}(\zeta) = -\frac{1}{\ln(\kappa)} [1 + \Omega(1 - \kappa^2)] - \frac{2}{3}\Omega + \sum_{n=1}^{\infty} A_n \exp\left(\frac{-\lambda^2 \zeta}{Gz}\right) \bar{F}_n(\lambda_n)$$

Eq. 5.2.25

The value of κ is between zero and one, and thus the natural logarithm in the first term cancels out the first negative. This ensures a positive, steady temperature profile. Eq. 5.2.25 can be used much like Eq. 5.1.52, in that it describes the development of temperature in the element as only a function of the axial direction.

In order to simulate the temperature profile in the extruder, the above solution methodology is applied on an element-wise basis. The temperature profiles developed in this chapter are used to approximate the temperature profile for both conveying and kneading elements. The exit temperature of one element is the initial condition for the next element. The calculation continues down the length of the extruder, and changes depending on the type and size of the element.

6. Comparisons and Future Work

6.1 Comparisons

The SSSP process is an alternative method of extrusion that has recently been applied to a variety of polymeric systems and successfully produced unique materials. A prescribed condition is that the process is performed on the material in its solid state; intense cooling with chillers and coolant lines is employed to remove the heat generated from the pulverizing action of the polymeric material. This balance between the internal heating and external cooling leads to an interesting heat transfer phenomenon. The goal of this thesis was to develop a mathematical model that describes the development of temperature within the extruder so that the heating and/or melting behavior of materials in an SSSP operation could be predicted.

Chapter 4 developed velocity profiles for material being processed in an SSSP instrument. These profiles describe individual screw elements, and are thus applied on an element-wise basis. The effective velocity profile that describe flow in conveying elements is written as

$$v_t(x') = \frac{2v_s}{(1+\varphi)} \frac{x'}{H} \quad \text{Eq. 4.1.40}$$

which describes the motion of material in a tilted Cartesian coordinate system. The tilt is associated with the flight angle of the screw, and is oriented such that the flow of material is in line with the z' -direction. The dimensionless form of Eq. 4.1.43 is written as

$$U(\xi') = \frac{2\xi'}{(1+\varphi)} \quad \text{Eq. 4.1.42}$$

where flow is pure drag induced flow. The velocity profile is linear, and specifically describes flow in starve-fed conveying elements.

In kneading elements, the velocity profiles are described by two orthogonal components. One is driven by drag, and one is driven by pressure.

$$v_{\theta,1} = \frac{\Omega_o}{r} \left[\frac{(r^2 - R_{i,1}^2)}{(1 - \kappa_1^2)} \right] \quad \text{Eq. 4.2.15}$$

$$v_{z,1} = -\frac{\Delta P_1 R_0^2}{\Delta L_1 4\mu} \left((1 - \kappa_1^2) \left[\frac{\ln\left(\frac{r}{R_0}\right)}{\ln(\kappa_1)} \right] - \left(1 - \frac{r^2}{R_0^2}\right) \right) \quad \text{Eq. 4.2.24}$$

The velocity field is thus deconstructed into a drag portion in θ and a pressure portion in ζ . In dimensionless form, the profiles can be written as

$$U_{\theta,1}(\gamma) = \frac{1}{\gamma} \left[\frac{(\gamma^2 - \kappa_1^2)}{(1 - \kappa_1^2)} \right] \quad \text{Eq. 4.2.29}$$

$$U_{\zeta,1}(\gamma) = -\beta_{k,1} \left((1 - \kappa_1^2) \left[\frac{\ln(\gamma)}{\ln(\kappa_1)} \right] - (1 - \gamma^2) \right) \quad \text{Eq. 4.2.31}$$

The above velocity profiles gave insight into the behavior of flow within the extruder, and were used in the derivation of temperature profiles. Chapter 5 provides the solution for temperature profiles. There is variation of temperature through both the channel height and the axial direction, but the profile is averaged through the former, and presented solely as a function of the latter. Temperature in conveying elements can be calculated using

$$\bar{\theta}(\zeta') = \left(\frac{1}{2} + \frac{\Omega}{12} \right) + \sum_{n=1}^8 A_n \exp\left(\frac{-\lambda_n^2 \zeta'}{Gz}\right) \bar{F}_n(\lambda_n) \quad \text{Eq. 5.1.52}$$

The temperature profile for kneading elements is written in cylindrical coordinates as

$$\bar{\theta}(\zeta) = -\frac{1}{\ln(\kappa)} [1 + \Omega(1 - \kappa^2)] - \frac{2}{3}\Omega + \sum_{n=1}^{\infty} A_n \exp\left(\frac{-\lambda^2 \zeta}{Gz}\right) \bar{F}_n(\lambda_n)$$

Eq. 5.2.25

Eq. 5.2.25 is a function of ζ rather than ζ' , and the heat generation term considers two components of velocity rather than one (as is the case for conveying). Furthermore, the eigenfunctions for Eqs. 5.1.52 and 5.2.25 are different, as they depend on the individual velocity profiles for each screw.

Eqs. 5.1.52 and 5.2.25 therefore are the main tools with which we can build the temperature profile for the entire extruder. The calculation begins with the first element on the screw, closest to the motor. This element is *always* a conveying element, so every calculation will begin with applying Eq. 5.1.52. The initial temperature of the material is incorporated into the constant A_n , as given in Eq. 5.1.39. The calculation is completed for the first conveying element, and the temperature at $\zeta = 1$ (the end of the element) is used as the initial temperature for the next element in the screw. If the element is conveying then Eq. 5.1.52 is used and, if kneading, Eq. 5.2.25 is used. This process then continues down the length of the screw, and a temperature profile for the entire extruder is generated.

6.2 Future Work

Although individual screw profiles were developed in this thesis, a full extruder model was not compiled. Using MATLAB, a script should be written that performs these calculations. Screw configuration, geometry of each element, feed rate, screw speed, and

material properties are all taken as inputs to the code. This script can then use these inputs to predict and approximate profiles of temperature in SSSP. Predicting these profiles lends insight into the appropriate processing parameters for a given material.

Comparisons between experiment and model can then be made, and the accuracy of the model can be assessed. Experiments should then be performed that mimic the conditions input to the MATLAB code. Temperature probes are located along the SSSP barrel, and can measure the evolution of material temperature along the extruder.

Discrepancies between the model and experiments can arise from numerous places. For example, this thesis considered viscous dissipation as the only mechanism of heat generation in SSSP; however, depending on the material being processed, viscous dissipation may not capture the full effects of heat generation. Viscous dissipation characterizes the transformation of kinetic energy (i.e. flow energy) into heat, and is a volumetric process that occurs throughout a flowing system. Particle size reduction, where millimeter size-pellets are pulverized into micron scale flakes, can lead to large surface energy changes. Mechanochemical reactions such as chain scission and chain branching are known to occur within the extruder, and may contribute to energy dissipation due to the breaking and forming of chemical bonds. Another potentially important mechanism of heat generation is friction between powder particles. The current model considered those extra heat generation sources to be insignificant, but they should be investigated and incorporated into the generation term Ω as necessary. Including these heat generation mechanisms could improve the accuracy and robustness of the temperature profile in SSSP.

The development of a full extruder model and associated experiments are in progress currently, using polypropylene as a model material. Figure 6.2.1 shows the screw design used in these experiments.

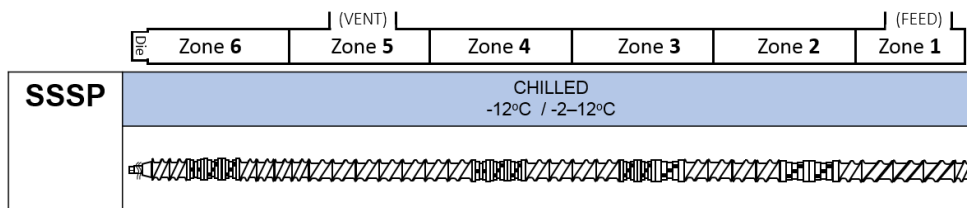


Figure 6.2.1: Screw design used in this study; mild configuration with four separate kneading zones

Large kneading elements are placed in Zone 2, and small kneading elements are placed in Zones 4 and 6. Both types of kneading elements are included in Zone 3, and no kneading elements are present in Zone 5.

Experiments have been conducted for varying flow rates and screw speeds, and the resulting temperature profiles are shown in Figures 6.2.2a and 6.2.2b.

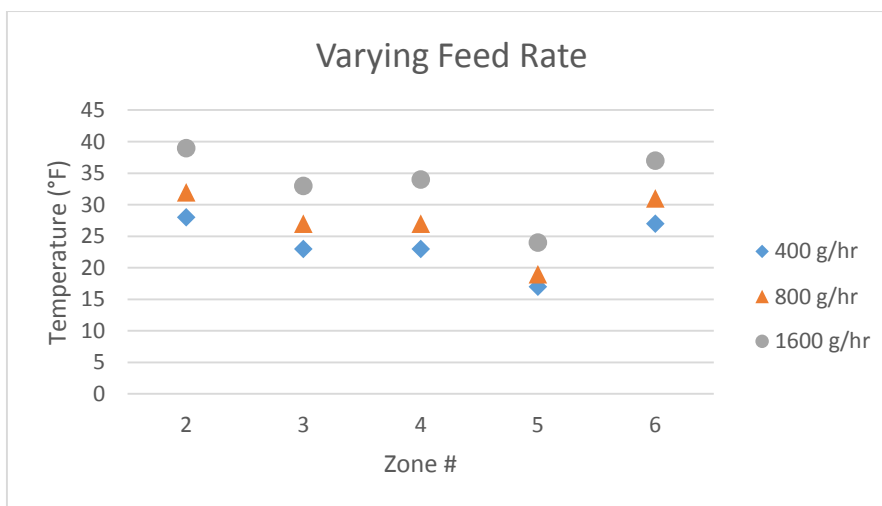


Figure 6.2.2a: Experimental temperature measurements for varying flow rates

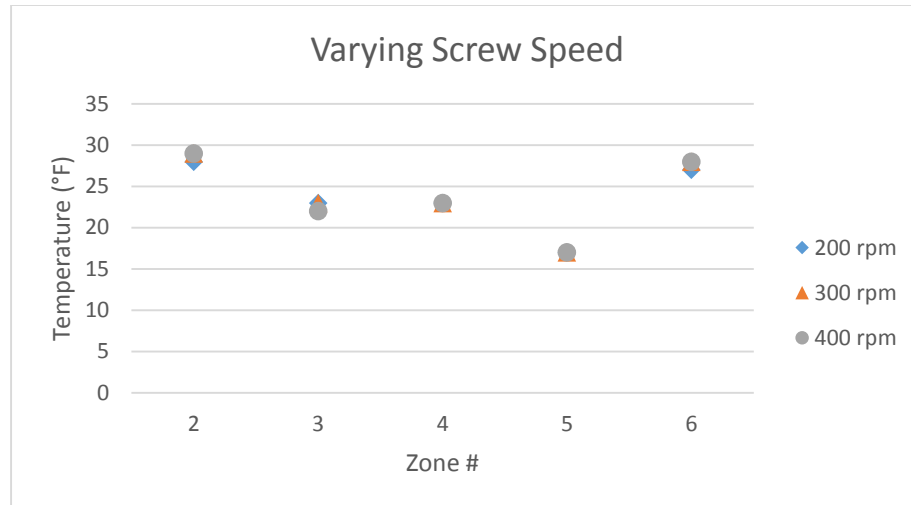


Figure 6.2.2b: Experimental temperature measurements for varying screw speeds

As can be seen, temperatures in the kneading zones (Zones 2, 3, 4, and 6) are higher than those in the conveying zone (Zone 5). The kneading zones are effectively heat sources, whereas the conveying zones are heat sinks. Increasing the flow rate of material is seen to increase temperature within the extruder, where increasing screw speed seems to have no effect.

The current iteration of the MATLAB code produces temperature profiles for SSSP; however, modeling varying feed rates and screw speeds produces results that do not behave realistically; the MATLAB code predicts temperatures of conveying zones that are higher than kneading zones. These results are shown in Figures 6.2.3a and 6.2.3b.

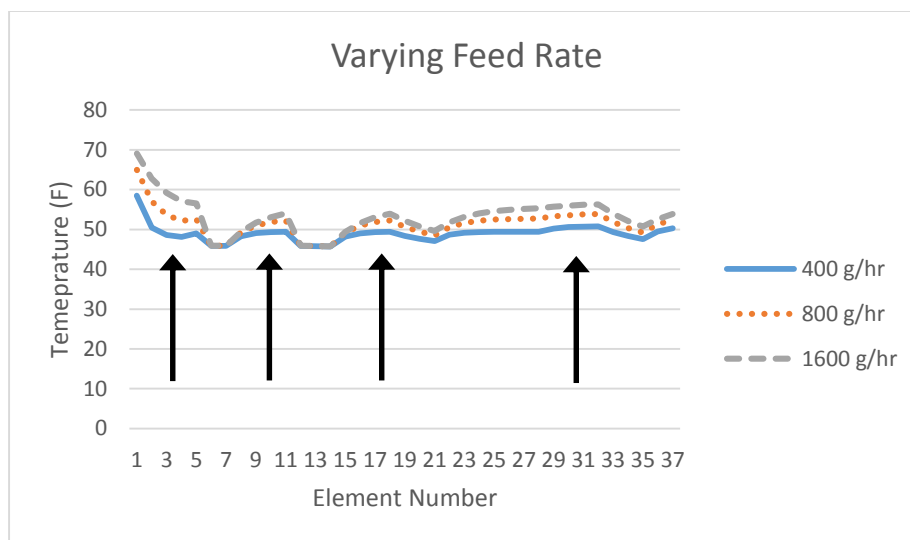


Figure 6.2.3a: Temperature predictions for various feed rates at 200 rpm; arrows point to kneading zones

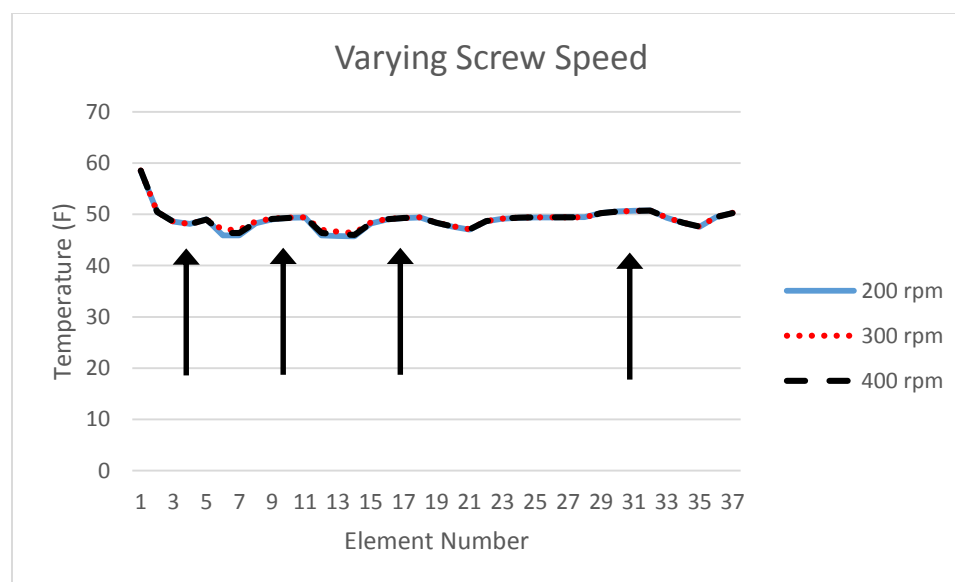


Figure 6.2.3b: Temperature predictions for varying screw speeds at 400 g/hr; arrows point to kneading zones

The current script correctly predicts increasing temperatures with increased flow rate; however, the increase in temperature is seen in the conveying elements, where

kneading elements are predicted to be flow rate invariant. The script also correctly predicts that temperatures are independent of screw speed, yet the issue of conveying temperatures versus kneading temperatures remains. Further modification to the MATLAB script is underway, with the goal of generating realistic and acceptable temperature profiles for a wide range of process parameters.

In summary, this study produces the foundation of a model that aims to predict temperatures in SSSP. Continuum mechanics and material balances are applied to solid-state extrusion in order to generate functions that could be used to approximate the development of temperature in SSSP. As SSSP is applied to different types of materials, these functions can be used to predict a feasible operating range for process parameters such as feed rate and screw speed. Trial-and-error practices common in current SSSP practices can be replaced by a numerical approximation, potentially leading to a more efficient design of experiments, as well as reducing the amount of wasted materials and energy.

References

- [1] Khait, K., & Torkelson, J. M. (1999). Solid-state shear pulverization of plastics: a green recycling process. *Polymer-Plastics Technology and Engineering*, 38(3), 445-457.
- [2] Lebovitz, A. H., Khait, K., & Torkelson, J. M. (2002). In situ block copolymer Formation during solid-state shear pulverization: an explanation for blend compatibilization via interpolymer radical reactions. *Macromolecules*, 35(26), 9716-9722.
- [3] Diop, M. F., & Torkelson, J. M. (2015). Novel synthesis of branched polypropylene via solid-state shear pulverization. *Polymer*, 60, 77-87.
- [4] Ganglani, M., Torkelson, J. M., Carr, S. H., & Khait, K. (2001). Trace levels of mechanochemical effects in pulverized polyolefins. *Journal of Applied Polymer Science*, 80(4), 671-679.
- [5] Whittington, A. M., Brouse, S. M., Malusis, M. A., & Wakabayashi, K. (2013). Efficient fabrication of polymer nanocomposites with effective exfoliation and dispersion by solid-state/melt extrusion. *Advances in Polymer Technology*, 32(1), 31334.
- [6] Lebovitz, A. H., Khait, K., & Torkelson, J. M. (2003). Sub-micron dispersed phase particle size in polymer blends: overcoming the Taylor limit via solid-state shear pulverization. *Polymer*, 44(1), 199-206.
- [7] Brunner, P. J., Clark, J. T., Torkelson, J. M., & Wakabayashi, K. (2012). Processing structure-property relationships in solid-state shear pulverization: parametric study of specific energy. *Polymer Engineering & Science*, 52(7), 1555-1564.
- [8] Lynch, B. B. (2014). The Crystallization Kinetics of Polylactic Acid (PLA) Processed Through Solid-State/Melt Extrusion. Bucknell University.
- [9] Wakabayashi, K., Pierre, C., Dikin, D. A., Ruoff, R. S., Ramanathan, T., Brinson, L. C., & Torkelson, J. M. (2008). Polymer-graphite nanocomposites: effective dispersion and major property enhancement via solid-state shear pulverization. *Macromolecules*, 41(6), 1905-1908.
- [10] Masuda, J., & Torkelson, J. M. (2008). Dispersion and major property

enhancements in polymer/multiwall carbon nanotube nanocomposites via solid-state shear pulverization followed by melt mixing. *Macromolecules*, 41(16), 5974-5977.

- [11] Khait, K., Carr, S. H., & Mack, M. H. (2001). *Solid-state Shear Pulverization: A New Polymer Processing and Powder Technology*. Technomic.
- [12] Miu, E. V., Fox, A. J., Jubb, S. H., & Wakabayashi, K. (2015). Morphology and toughness enhancements in recycled high-density polyethylene (rHDPE) via solid-state shear pulverization (SSSP) and solid-state/melt extrusion (SSME). *Journal of Applied Polymer Science*, 133(10), 43070.
- [13] Iyer, K. A., & Torkelson, J. M. (2014). Green composites of polypropylene and eggshell: effective biofiller size reduction and dispersion by single-step processing with solid-state shear pulverization. *Composites Science and Technology*, 102, 152-160.
- [14] Diop, M. F., Burghardt, W. R., & Torkelson, J. M. (2014). Well-mixed blends of HDPE and ultrahigh molecular weight polyethylene with major improvements in impact strength achieved via solid-state shear pulverization. *Polymer*, 55(19), 4948-4958.
- [15] White, J. L., Coran, A. Y., & Moet, A. (2001). *Polymer Mixing: Technology and Engineering*. Hanser Verlag.
- [16] Sakai, T. (2013). Screw extrusion technology—past, present and future. *Polimery*, 58(11-12), 847-857.
- [17] Tadmor, Z., & Gogos, C. G. (2013). *Principles of Polymer Processing*. Wiley.
- [18] No. 5 - Twin-Screw Extrusion: Plastics Technology. *Plastics Technology Magazine and Newsletter*, Oct. 2005.
- [19] Colombo, R. Screw Press for Mixing and Extruding Plastic Materials. Roberto Colombo, assignee. Patent US 2543894 A. 6 Mar. 1951.
- [20] Schonfeld, S. Information Presented by Coperion. AIChE National Conference 2016.
- [21] Villmow, T., Pötschke, P., Pegel, S., Häussler, L., & Kretzschmar, B. (2008). Influence of twin screw extrusion conditions on the dispersion of multi-walled carbon nanotubes in a poly (lactic acid) matrix. *Polymer*, 49(16), 3500-3509.

- [22] Villmow, T., Kretzschmar, B., & Pötschke, P. (2010). Influence of screw configuration, residence time, and specific mechanical energy in twin-screw extrusion of polycaprolactone/multi-walled carbon nanotube composites. *Composites Science and Technology*, 70(14), 2045-2055.
- [23] Huneault, M. A., Champagne, M. F., & Luciani, A. (1996). Polymer blend mixing and dispersion in the kneading section of a twin-screw extruder. *Polymer Engineering & Science*, 36(12), 1694-1706.
- [24] Furgiuele, N., Lebovitz, A. H., Khait, K., & Torkelson, J. M. (2000). Novel strategy for polymer blend compatibilization: solid-state shear pulverization. *Macromolecules*, 33(2), 225-228.
- [25] Furgiuele, N., Lebovitz, A. H., Khait, K., & Torkelson, J. M. (2000). Efficient mixing of polymer blends of extreme viscosity ratio: elimination of phase inversion via solid-state shear pulverization. *Polymer Engineering & Science*, 40(6), 1447-1457.
- [26] Felder, R. M., & Rousseau, R. W. (2004) *Elementary Principles of Chemical Processes*. Wiley.
- [27] Tao, Y., Lebovitz, A. H., & Torkelson, J. M. (2005). Compatibilizing effects Of block copolymer mixed with immiscible polymer blends by solid-state shear pulverization: stabilizing the dispersed phase to static coarsening. *Polymer*, 46(13), 4753-4761.
- [28] Bird, R. B., Stewart, W. E., & Lightfoot, E. N. (2007). *Transport Phenomena*. Wiley.
- [29] Rauwendaal, C., & Housz, J. I. (1990). Temperature development in pure drag flow, exact analytical solution. *Journal of Reinforced Plastics and Composites*, 9(6), 583-601.
- [30] Chen, Z., & White, J. L. (1994). Simulation of non-isothermal flow in twin screw extrusion: modular co-rotating intermeshing twin screw compounding extrusion system with multiple feeds and vents. *International Polymer Processing*, 9(4), 310-318.
- [31] Chiruvella, R. V., Jaluria, Y., Karwe, M. V., & Sernas, V. (1996). Transport in a twin-screw extruder for the processing of polymers. *Polymer Engineering & Science*, 36(11), 1531-1540.
- [32] "Continuum Mechanics/Motion and Displacement." – Wikiversity.

- [33] Bawiskar, S., & White, J. L. (1998). Melting model for modular self wiping co-rotating twin screw extruders. *Polymer Engineering & Science*, 38(5), 727-740.
- [34] Suk, D. (2001). Modeling heat transfer in screw extrusion with special application to Modular self-wiping co-rotating twin-screw extrusion. *Polymer Engineering & Science*, 41(8), 1448-1455.
- [35] Denson, C. D., & Hwang, B. K. (1980). The influence of the axial pressure gradient on flow rate for Newtonian liquids in a self wiping, co-rotating twin screw extruder. *Polymer Engineering & Science*, 20(14), 965-971.
- [36] Vergnes, B., Valle, G. D., & Delamare, L. (1998). A global computer software for polymer flows in corotating twin screw extruders. *Polymer Engineering & Science*, 38(11), 1781-1792.
- [37] Mark, J. E. (1996) *Physical Properties of Polymers Handbook*. AIP.
- [38] Jakob, M. (1949). *Heat Transfer*. Wiley.
- [39] Hildebrand, F. B. (1976). *Advanced Calculus for Applications*. Prentice Hall.

Appendix A: Discussion of Pressure Effects on Velocity and Temperature Profiles

A.1 Development of Velocity Profiles for Various Pressure Effects

A new scale variable is introduced here as

$$\beta = \frac{\frac{\Delta P H^2}{2\mu L}}{v_s} = \frac{\text{pressure flow in negative } z}{\text{drag flow in positive } z} \quad \text{Eq. A.1.1}$$

This dimensionless group characterizes pressure induced flow in the negative z -direction versus drag induced flow in the positive z -direction [17]. It is for Cartesian systems. A cylindrical version of this group can be written as

$$\beta_{k,j} = \frac{\frac{\Delta P_j R_0^2}{\Delta L_j^4 \mu}}{v_s} \quad \text{for } j = 1, 2 \text{ and where } v_s = \Omega_o r \quad \text{Eq. 4.2.28}$$

Larger values of β indicate larger pressure effects within the system. Figure A.1.1 shows the dimensionless velocity profile, $U(\xi)$, for several values of β .

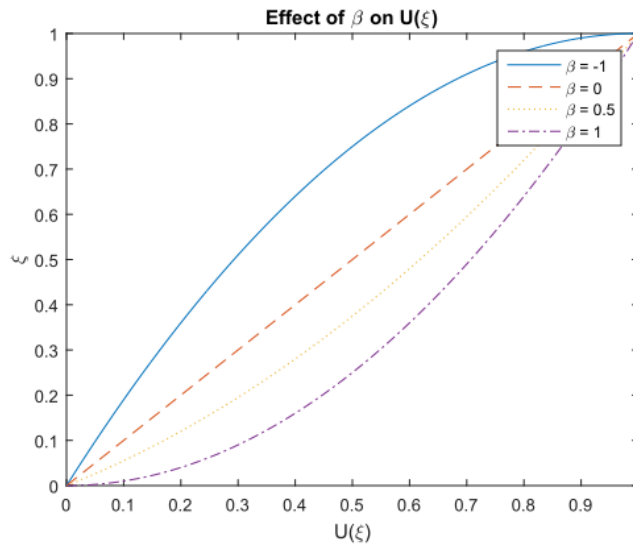


Figure A.1.1: Dimensionless velocity profiles for various values of β

As can be seen, larger values of β develop larger amounts of backflow within the channel. Negative values of β instigate forward flow. The case of $\beta = 1$ is of particular interest, as this is the largest value of β which exhibits no negative flow in the entirety of the channel.

Applying the appropriate scale variables to Eqs. 4.1.21 and 4.1.23, the dimensionless velocity profiles for Zone 1 and Zone 2 are

$$U(\xi) = \xi' - \beta(\xi' - \xi'^2) \quad \text{for Zone 1} \quad \text{Eq. A.1.2}$$

$$U(\xi) = \xi' - 2\beta(\xi' - \xi'^2) \quad \text{for Zone 2} \quad \text{Eq. A.1.3}$$

A.2 Development of Temperature Profiles for Various Pressure Effects

For the case of $\beta = 1$, there exists another analytical solution for the temperature profile in a screw element (the analytical solution for the case of $\beta = 0$ is presented in Section 5.1). Using the value of $\beta = 0$ for $U(\xi')$ in Eq. 5.1.36 gives

$$\frac{d^2 X(\xi')}{d\xi'^2} + \lambda^2 \xi'^2 X(\xi') = 0 \quad \text{for } \beta = 1 \quad \text{Eq. A.2.1}$$

The same approach of using Eq. 5.1.44 to generate a Bessel function solution is applied here, and gives

$$\theta(\xi', \zeta') = (1 - \xi') \left(1 + \frac{\Omega}{2} \xi' \right) + \sum_{n=1}^{\infty} A_n \exp\left(\frac{-\lambda_n^2 \zeta'}{Gz}\right) \sqrt{\xi'} J_{\frac{1}{4}}\left(\frac{1}{2} \lambda_n \xi'^2\right) \quad \text{Eq. A.2.2}$$

The constants A_n are given in table A.2.1.

Table A.2.1: First eight eigenvalues and corresponding constants

$\beta = 1$		
n	λ_n	A_n
1	5.56178...	0.4946...
2	11.81229...	-1.0223...
3	18.08477...	0.4456...
4	24.36268...	-0.8157...
5	30.64274...	0.4149...
6	36.92385...	-0.7181...
7	43.20557...	0.3938...
8	49.48765...	-0.6571...

The first eight eigenfunctions are then given in Figure A.2.1.

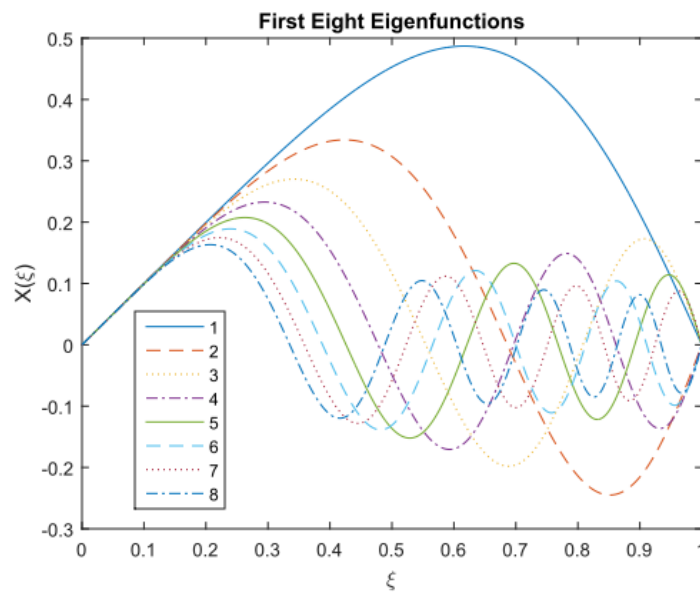


Figure A.2.1: First eight eigenfunctions that contribute to the series solution for $X(\xi')$ for $\beta = 1$

As in Section 5.1, the sum of these eigenfunctions is shown in Figure A.2.2

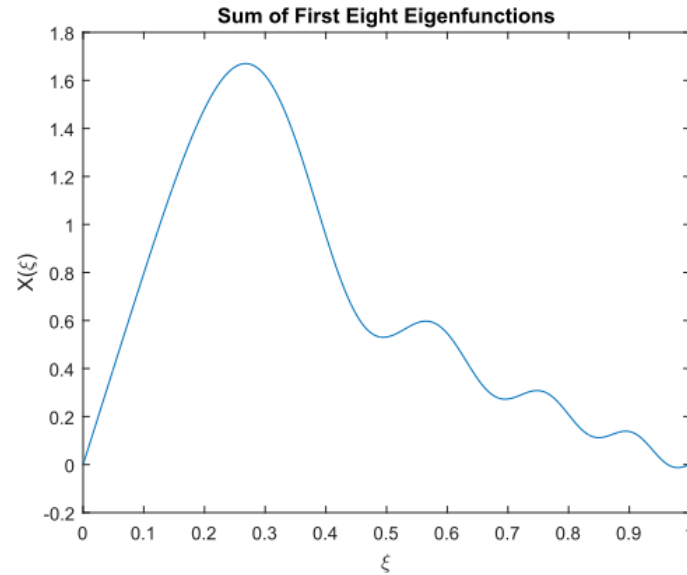


Figure A.2.2: $[\sum_{n=1}^8 A_n F_n(\lambda_n; \xi')]$ Sum of the first eight eigenfunctions that contribute to the solution for $X(\xi')$ for $\beta = 1$

The averaged eigenfunction series is shown here in Figure A.2.3. The same averaging suggested in Section 5.1 is used here to calculate the averaged eigenfunctions $\bar{F}_n(\lambda_n)$.

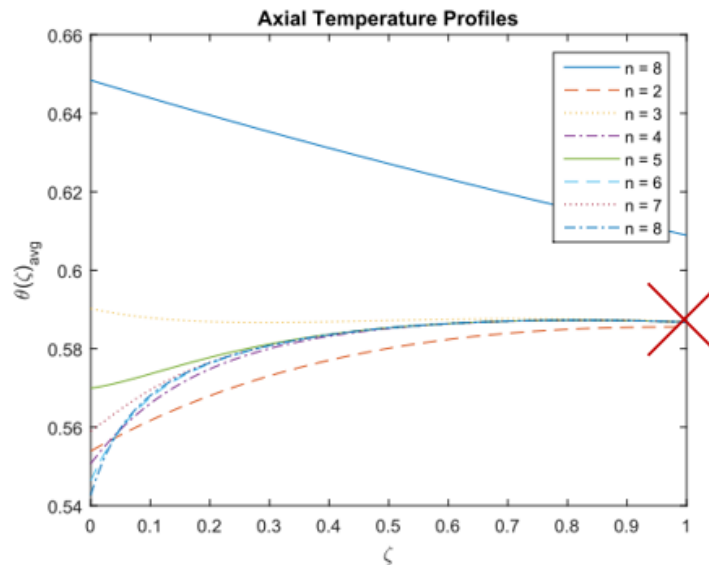


Figure A.2.3: Comparison of the effectiveness of various series solutions for $\beta = 1$

These averaged solutions are similar to those for the case of $\beta = 0$. The discussion in this appendix presents the application of the same solution methodology used in Chapter 5 to the limiting case of pressure driven flow in conveying elements. Flow in standard SSSP operation is expected to be starve fed, so the results given in Section 5.1 are more applicable.

Appendix B: Discussion of Heat Generation, Ω

The variable Ω represents the generation of heat within SSSP. It is written explicitly as

$$\Omega = \frac{S_c H^2}{k[T_s - T_b]} \psi \quad \text{Eq. B.1}$$

where S_c is some scale heat generation, H is the channel height, k is thermal conductivity, T_s is the screw temperature, T_b is the barrel temperature, and ψ is dimensionless heat generation. Eq. 5.1.10d allows us to write Eq. B.1 as

$$\Omega = \frac{S H^2}{k[T_s - T_b]} \quad \text{Eq. B.2}$$

where S is *dimensional* heat generation. This term can be represented by viscous dissipation, chemical reaction, etc. Any process that generates heat can be incorporated into S . This development considers viscous dissipation as the only source of heat generation in SSSP. This can be written as $\eta \Phi_v$, where Φ_v is a function of the velocity gradients (shear) in the system. This allows us to write *dimensionless* heat generation as

$$\Omega = \frac{H^2}{k[T_s - T_b]} \eta \Phi_v \quad \text{Eq. B.3}$$

All of the values on the right hand side of Equation B.3 are known, therefore Ω can be calculated. Ω is a balance of heat generation and heat conduction through the system.